Research Square

Preprints are preliminary reports that have not undergone peer review.
They should not be considered conclusive, used to inform clinical practice,
or referenced by the media as validated information.

Hydrologic pathway controls on surface and groundwater nutrient delivery under agricultural fallow and crop rotation in the Fuxian Lake watershed

Tingyu Ren
Dali Rays Computational Intelligence Lab
Xing Chen
Dali Rays Computational Intelligence Lab
Ziguan Wang
lanaya8155@outlook.com

China University of Geosciences Beijing
Xiaolu Li
Dali Rays Computational Intelligence Lab
Xiaoling Zhang
Dali Rays Computational Intelligence Lab
Wenjing Ma
Dali Rays Computational Intelligence Lab
Rui Zou
Dali Rays Computational Intelligence Lab

Research Article

Keywords: Agricultural nonpoint source pollution, Fallow and crop rotation, Surface water–groundwater exchange, Integrated watershed–groundwater–lake modeling, Pathway attribution, Fuxian Lake watershed

Posted Date: July 8th, 2026

DOI: https://doi.org/10.21203/rs.3.rs-9999753/v1

License: This work is licensed under a Creative Commons Attribution 4.0 International License.
Read Full License

Additional Declarations: No competing interests reported.

Hydrologic pathway controls on surface and groundwater nutrient delivery under agricultural fallow and crop rotation in the Fuxian Lake watershed

Tingyu Ren[1,2,4], Xing Chen[1,2,4], Ziguan Wang[3]* Xiaolu Li[1,2], Xiaoling Zhang[1], Wenjing Ma[1], Rui Zou[1,2]*

[1]Dali Rays Computational Intelligence Lab, Dali 671000, China.

[2] Beijing Inteliway Environmental Co. Ltd., Beijing 100085, China.

[3] Research Institute of Nature & Culture, China University of Geosciences (Beijing), Beijing 100083, China

[4]These authors contributed equally to the work: Tingyu Ren, Xing Chen.

*Corresponding author at Research Institute of Nature & Culture, China University of Geosciences (Beijing), Beijing 100083, China, e-mail address: rz5q2008@gmail.com , tel: +86 18288246985.

Tingyu Ren: tingyu_ren@outlook.com

Xing Chen: xing.chen@alumni.duke.edu

Ziguan Wang:lanaya8155@outlook.com

Xiaolu Li: 314157550@qq.com

Xiaoling Zhang:zhangxiaoling@pku.edu.cn

Wenjing Ma: xiashangshu@163.com

Abstract:

Deep oligotrophic lakes can face water-quality risks when long-term agricultural nonpoint loading coincides with strong monsoon transport. We quantified the effects of farmland fallow on inflow loads to Fuxian Lake using an integrated watershed – groundwater – lake modeling framework constrained by multi-media monitoring and evaluated via consistent pre- (2014 – 2017) and post-implementation (2018 – 2020) accounting. Baseline mean inflow loads were 2601.75 t yr−1 for chemical oxygen demand (CODCR), 84.13 t yr−1 for ammonium-N (NH4 – N), 590.48 t yr−1 for total nitrogen (TN), and 53.13 t yr−1 for total phosphorus (TP). In the ring-lake zone, groundwater inflow decreased from 12.3 to 10.0 million m^3 yr^{-1}, and groundwater-borne TN declined from 183.0 to 110.0 t yr^{-1}, indicating a substantial weakening of nearshore subsurface nitrogen supply after fallowing. At the watershed scale, mean reductions strengthened with the assessment horizon: TN and TP reductions increased from 4.63% and 2.82% over a 3-year window to 15.55% and 7.21% over 7 years, consistent with cumulative benefits rather than a short-lived response. Seasonal targeting was effective, with wet-season (summer) fallow reducing TN by 35.7% and TP by 31.9%. Spatial extent controlled the maximum achievable reductions, with whole-cropland fallow producing the deepest decreases in TN and TP, reaching 52.4% and 50.4%, respectively. Overall, the pre – post comparison and mode-to-mode contrasts indicate that fallow outcomes depend jointly on timing and spatial coverage, while pathway accounting suggests reduced groundwater leaching and a residual load structure that is relatively more dominated by surface runoff.

Keyword: Agricultural nonpoint source pollution; Fallow and crop rotation; Surface water – groundwater exchange; Integrated watershed – groundwater – lake modeling; Pathway attribution; Fuxian Lake watershed

1. Introduction

Water-quality degradation in lakes is rarely driven by a single in-lake process that can be isolated and reversed. Instead, it typically emerges from the combined effects of long-term external loading

from the watershed and hydrologic transport that mobilizes and delivers pollutants to the lake (Aboelnour et al., 2023; Lintern et al., 2020). For deep lakes where nitrogen and phosphorus are the primary limiting factors, persistent external inputs can erode self-purification capacity and ecological resilience, while high-rainfall or high-flow periods amplify fluctuations in water quality and increase the risk of algal blooms (Husk et al., 2024; Liu et al., 2024) .In recent decades, an integrated "watershed-to-lake" perspective has increasingly shaped lake management practice: (Chao et al., 2023; Cheng et al., 2025; Liu et al., 2024): effective restoration requires not only reducing pollutant generation at the source, but also clarifying how pollutants are mobilized, routed through different hydrologic pathways, and ultimately delivered to the receiving water (Wan et al., 2023; Zhou et al., 2024). Consequently, building an interpretable, accountable, and verifiable evidence chain for reductions in lake-bound loads has become a cornerstone for moving lake management from engineering-driven interventions toward refined, performance-oriented governance (Liu et al., 2025; Trang et al., 2025).

Within watershed load control strategies, agricultural nonpoint-source pollution is widely recognized as a major contributor to nitrogen and phosphorus inputs (Peng et al., 2022; Wang et al., 2023; Zhao et al., 2023). Fallowing and crop rotation, as forms of cropping-system adjustment, have been implemented in many regions to reduce input intensity, alter the activity of soil nutrient pools, and modify runoff generation and infiltration by changing ground cover and soil physical structure.(Bonab and Nayyer, 2020; Mehdi-Schulz et al., 2025; Ramião et al., 2024) . However, a pronounced gap remains in existing research and practice-oriented assessments. Many evaluations emphasize changes in total loads before and after implementation but provide limited mechanistic interpretation of the hydrologic pathways responsible for those changes. As a result, comparable load reductions are often difficult to reproduce across regions or to generalize across management configurations. For decision-making, the critical questions extend beyond whether loads decline.

Managers must determine whether observed reductions are driven primarily by decreased source strength or by altered delivery capacity, whether the dominant reductions occur via surface runoff, interflow or groundwater pathways, and whether compensatory shifts among pathways lead to a structural reorganization of contributions. Without such information, optimization of intervention portfolios tends to remain at a coarse "effective versus ineffective" level, making it difficult to establish stable priorities and a sustainable trajectory for load reduction. Quantitatively attributing loads to distinct pathways and media is therefore essential for decision-making: it enables managers to identify where reductions are actually realized, avoid "apparent improvements" caused by pathway switching, and allocate limited resources to interventions with verifiable, long-term effectiveness.

A central methodological issue is that surface runoff and groundwater are not independent conduits. Changes in cropping systems and land management primarily alter source strength, especially fertilizer application rates and the size and lability of soil nutrient pools, rather than fundamentally reorganizing watershed hydrology. Any hydrologic implications, if present, are more plausibly mediated by management-related practices such as irrigation scheduling, drainage operations, and field water control associated with different crop types and rotations. Groundwater is not only a water-flux pathway but also a carrier of dissolved nitrogen species, where storage and lag effects can sustain background inputs over extended periods, including during dry seasons. In contrast, surface processes are often event-driven and can intensify particulate transport and phosphorus export during storms. If assessments rely only on river cross sections or a single environmental medium, reductions in one pathway may be overstated, while compensating contributions from another pathway remain hidden, weakening the targeting and interpretability of management decisions (Kujawa et al., 2022; Sharma et al., 2023; Venishetty et al., 2024).

Accordingly, current evaluations of agricultural measures such as fallowing and crop rotation exhibit at least three major research gaps that require systematic methodological advances. First, there is a lack of quantitative interaction-coupling frameworks that explicitly integrate surface-water and groundwater processes for the purpose of assessing management interventions. Many studies still estimate loads from surface runoff and groundwater separately, or simplify groundwater as a fixed baseflow term, making it difficult to represent how changes in infiltration and recharge induced by cropping-system adjustment propagate through groundwater systems and further influence baseflow, nearshore exchange, and lake delivery. This also limits the ability to interpret pathway reorganization within a single conservation-based accounting framework (Chang et al., 2023; Wei et al., 2024). Second, there remains a shortage of evaluation paradigms that constrain water-quality assessments with water-balance consistency (Biagi et al., 2022; Bodrud-Doza et al., 2025; Zhou et al., 2024). Because loads are jointly determined by concentration and discharge, comparisons based solely on concentration or solely on load can obscure key mechanisms, particularly when interventions simultaneously alter runoff generation and infiltration (Miller et al., 2021; Wu and Chen, 2024). Robust inference requires synchronized accounting of hydrologic fluxes and constituent transport, supported by explicit pathway decomposition within a consistent water-balance structure (He et al., 2023; Mooney et al., 2020; Wan et al., 2023). Third, evaluations of intervention effectiveness are often constrained by fragmented evidence across media and by a lack of operational attribution frameworks that can translate modeling outputs into verifiable management signals (Kujawa et al., 2022). Many studies report before and after changes at monitoring sections or within a single medium, yet do not explicitly decompose where reductions are realized (surface water, groundwater, or internal storage) and whether observed improvements reflect a true net reduction or a redistribution among pathways (Husk et al., 2024; Ramião et al., 2024). A method that couples process-aware modeling with pathway-resolved accounting and

consistent evaluation metrics can strengthen quantifiable assessment of intervention outcomes, thereby improving decision support and priority setting (Venishetty et al., 2024).

These overarching gaps are compounded by several practical bottlenecks in evaluating fallowing and crop rotation. Source-strength changes and delivery-capacity changes often occur simultaneously. Fallowing may reduce agricultural inputs and modify soil nutrient pools, while also altering ground cover and infiltration conditions, so that load responses are jointly controlled by source terms and pathway terms. In addition, different pollutants behave differently across pathways: dissolved nitrogen is more likely to be transported through groundwater and interflow, whereas phosphorus is often associated with particulates and surface erosion processes. Without joint multi-constituent accounting and pathway decomposition, assessments risk inferring watershed-wide effectiveness from a single indicator. Finally, nearshore exchange processes are highly heterogeneous in space, and groundwater inflow to lakes is frequently estimated with empirical assumptions unless supported by coupled models and monitoring constraints, limiting fine-scale management and scenario optimization.

Fuxian Lake provides a representative and urgent application setting for these scientific and management challenges. As a typical deep lake, Fuxian Lake reaches a maximum depth of approximately 158.9 m, stores about 20.62 billion m^3 of water, and accounts for about 68.3% of the total storage of the nine plateau lakes in Yunnan Province, highlighting its exceptional scarcity and strategic value. In recent years, the lake has generally maintained Class I water quality, yet total nitrogen has increased and approached the Class I threshold; the mean lake concentration reached 0.2 mg/L in 2018, touching the Class I limit. Meanwhile, noncompliance among major inflowing rivers remains prominent: some channels persistently fall into inferior Class V, and multiple inflows still fail to meet inflow standards, indicating that the management challenge is

both severe and persistent. In terms of source structure, agricultural nonpoint-source pollution is considered an important contributor to watershed nitrogen and phosphorus loads, and the expansion of high-fertilizer, high-irrigation vegetable production in the plain areas has further intensified nonpoint-source pressures. To control agricultural nonpoint-source pollution and protect Fuxian Lake, a farmland fallowing program was formulated in 2017 with phased implementation pathways and explicit targets for reductions in total nitrogen and total phosphorus, signaling a transition from general advocacy to goal-constrained and performance-oriented load management. Under this context, if an assessment cannot answer where lake-bound loads originate, through which pathways reductions occur, and whether pathway contributions are reorganized, it cannot credibly support decisions on the scale and configuration of fallowing, nor can it adequately address the practical tradeoffs between water-quality protection and regional development.

Against this backdrop, the central question addressed in this study is as follows: under cropping-system adjustments such as fallowing and crop rotation, how can an evaluation system be constructed that unifies surface and subsurface processes within a single mass-conservation framework, enabling synchronized quantification of water allocation, pathway switching, and nitrogen and phosphorus transport, and allowing mechanism-interpretable and verifiable identification of effects through implementation–control comparison. Emphasizing surface–groundwater unity is essential because the water-quality benefits of fallowing and rotation cannot be reliably evaluated by a single medium or a single process in isolation. Instead, a watershed-system perspective is required that couples watershed hydrologic and water-quality processes, groundwater–surface-water exchange, and the lake's internal hydrodynamic and water-quality responses. Specifically, three operational scientific questions are addressed. First, we establish the credibility of the modeling framework by quantitatively evaluating simulation–observation agreement for key hydrologic and water-quality variables, reporting performance and errors in a

transparent manner to support interpretable inference. Second, using a consistent scenario design, we quantify the magnitude of load reductions attributable to fallowing and rotation by comparing pre-intervention and post-intervention periods, providing effect sizes that directly reflect management-relevant improvements. Third, we further quantify and rank the incremental load-reduction benefits of alternative fallowing measures, enabling evidence-based prioritization of intervention portfolios toward sustained nitrogen and phosphorus reduction.

2 Methods

2.1 Study Area Overview and Sampling Design

The Fuxian Lake watershed is located in the central Yunnan Plateau, Yunnan Province, China, with geographic coordinates of 24.35°–24.63° N and 102.82°–102.97° E (Figure 1). The watershed covers an area of approximately 477 km² and features a south–high to north–low topographic gradient dominated by plateau mountains and hills. Elevation ranges from 1612 to 2774 m, yielding a relative relief of 1162 m. Steep slopes are widespread (slopes >20° account for ~24% of the watershed area), while gentler cultivated slopes are mainly distributed in the lakeside basin/terrace zone (slopes <10° account for ~40%). The region has a subtropical monsoon climate, with a mean annual temperature of ~15.5 °C and mean annual precipitation of ~950 mm. Approximately 80–85% of rainfall occurs during the wet season from May to October. Fuxian Lake is a deep-water lake at the center of the watershed, with a lake-surface elevation of ~1723 m, an area of 216.6 km², a mean depth of ~95 m, and a maximum depth of 158 m. It is the third deepest freshwater lake in China and has long remained in an oligotrophic state. More than 20 short rivers/streams flow into the lake, and the lake has only one surface outflow—the Haikou River—located along the mid-eastern shore. Land use is dominated by forests and croplands: forest (including shrubland) accounts for ~44% of the area, while cropland (e.g., dryland and paddy fields) accounts for ~33%;

198 the remainder consists of grassland, towns/villages, water bodies, and other land covers.
199 Agricultural activities are concentrated in the relatively flat ring-lake basin zone, where major crops
200 include rice, maize, vegetables, and cash crops. Over-fertilization and cropland expansion over
201 recent decades have increased non-point source pollution pressure, threatening lake water quality.

202 To evaluate the impacts of agricultural measures (e.g., fallow and crop rotation) on watershed
203 inflow water quality, this study conducted synchronous, multi-media and multi-site monitoring in
204 the Fuxian Lake watershed during 2018–2020. Specifically, eight surface-water monitoring
205 sections were established on major inflow rivers (Liangwang River, Fucheng River, Dufang Dagou,
206 Dongda River, Daicun River, Dajiyu River, Jianshan River, and Shanchong River). River water
207 samples were collected monthly from June 2018 to June 2020 (37 campaigns), resulting in 299
208 samples. Monitored indicators included total nitrogen (TN), total phosphorus (TP), chemical
209 oxygen demand (CODCR), and other nutrient/organic pollution metrics (Fig.1).

210 For groundwater, seven monitoring wells were deployed along the lakeshore and in the basin
211 zone (e.g., Guangnanying, Siji Farm, Guoziyuan, Xilongtan, Xipu Park, Heshang Village, and
212 Daqiansuo), complemented by sampling from several agricultural irrigation wells. Groundwater
213 was sampled monthly from March 2019 to June 2020, yielding more than 550 samples, and nutrient
214 concentrations were analyzed to characterize groundwater quality dynamics. In addition, 44 small
215 runoff monitoring plots were established within fallow pilot areas in key agricultural zones around
216 the lake to enable in situ observations of runoff, sediment yield, and nitrogen/phosphorus losses
217 under different land uses and management practices. Each plot (tens of square meters) represented
218 a specific crop or fallow regime and was equipped with devices such as collecting troughs and soil
219 lysimeters to capture surface runoff and percolation/leachate. Seven land-use/management modes
220 were included: vegetable cultivation, flue-cured tobacco cultivation, blueberry cultivation, vetiver
221 cultivation, rice–lotus cultivation, ecological nursery cultivation, and complete fallow. Each mode

included five spatially independent replicate plots. High-frequency monitoring was conducted from June 2018 to June 2020: runoff and leachate samples were collected for major rainfall events, and stratified soil samples were collected every six months at depths of 0–20 cm, 20–40 cm, 40–60 cm, and 60–80 cm to capture temporal dynamics in soil nutrient pools. Figure 1 shows the study area and the spatial distribution of monitoring sites, including Fuxian Lake and major inflow rivers, the locations of fallow pilot areas, surface-water sampling sections, groundwater monitoring wells, and runoff plots (with inset maps showing the locations of Yunnan Province and the watershed) (Figure 1).

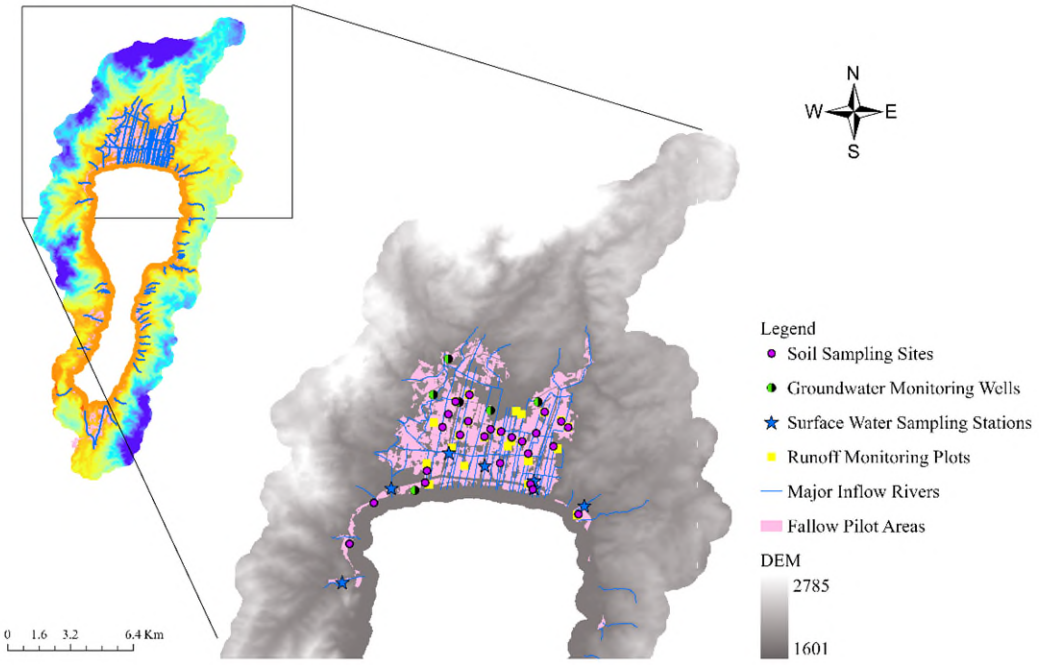


Figure 1. Study area, soil sampling sites, groundwater monitoring wells, surface water sampling stations, runoff monitoring plots, major inflow rivers and fallow pilot areas.

2.2 Model Structure and Evaluation Framework

We developed an integrated "watershed–groundwater–lake" hydrology–water quality modelling and assessment system to quantify how fallow management alters pollutant loads delivered to the lake and how these load changes propagate into lake water-quality responses. The overall

architecture and computational workflow are summarized in Figure 2. The system couples three process-based modules that represent: (1) watershed rainfall–runoff generation, non-point source pollutant production, and river-network delivery; (2) groundwater recharge, variably saturated subsurface transport, and exchange fluxes with rivers and the lake; and (3) lake hydrodynamics and biogeochemical water-quality dynamics.

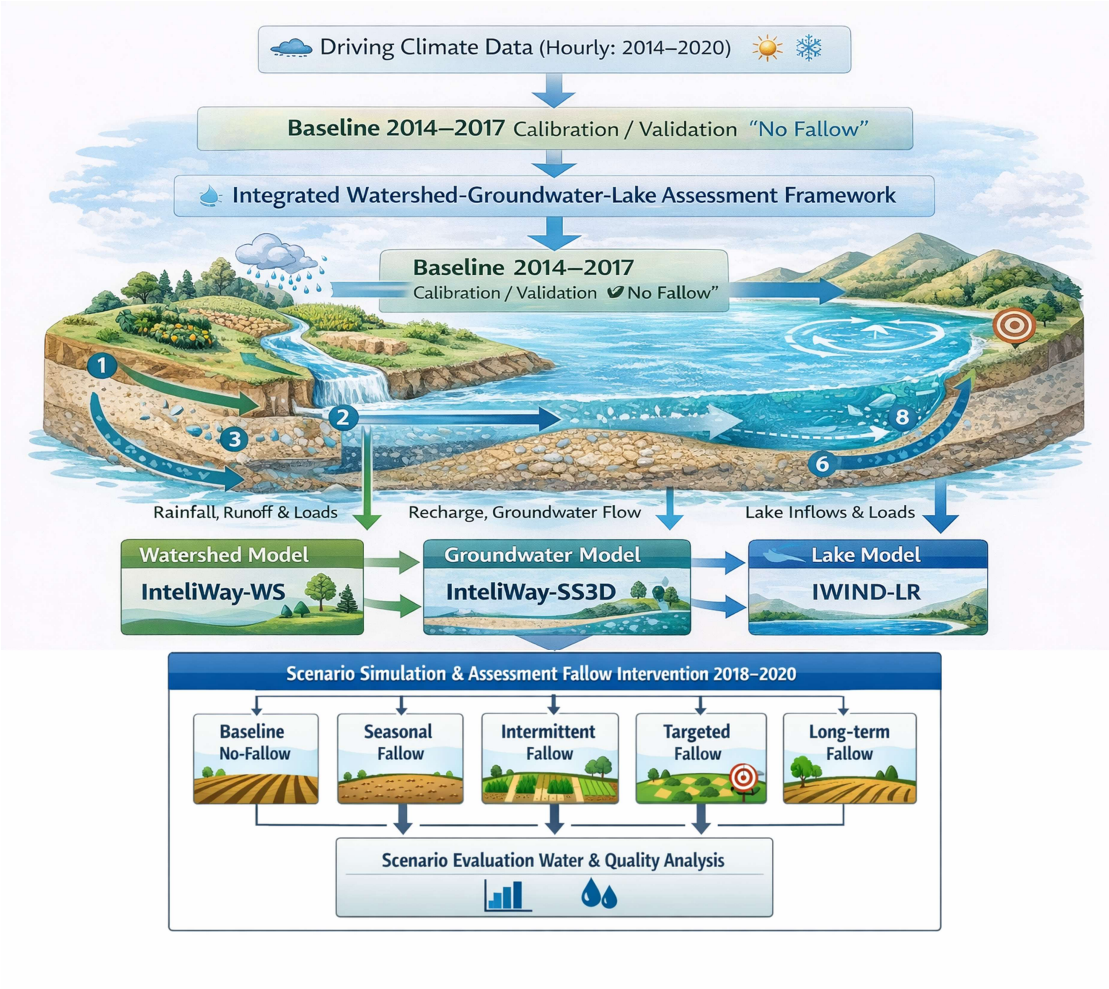


Figure 2. Flowchart and methodology of this study

The integrated system was driven by continuous, watershed-scale simulations forced by hourly meteorological time series covering 2014–2020. A baseline period (2014–2017; pre-fallow) was simulated to characterize reference hydrological conditions and pollutant loading to the lake, followed by scenario simulations for 2018–2020 in which alternative fallow strategies were

implemented to quantify load reductions. The three modules were configured with consistent temporal resolution and explicit spatial coupling to enable the exchange of fluxes and concentrations across model boundaries, forming a coherent dynamic chain of "rainfall–runoff–infiltration–groundwater flow–lake inflow–water-quality response". The watershed module employs InteliWay-WS (Beijing Innowater Environmental Technology Co., Ltd.), which inherits from and extends the U.S. EPA semi-distributed watershed model LSPC. InteliWay-WS adopts a "subwatershed–HRU (hydrologic response unit)" representation to simulate rainfall–runoff processes, soil-water balance, and the generation and routing of non-point pollutants (e.g., nitrogen and phosphorus) through the landscape and stream network. Relative to conventional LSPC applications that commonly prescribe fertilization inputs using coarse temporal averages and rely on simplified build-up/wash-off descriptions for agricultural non-point processes, InteliWay-WS incorporates enhanced agricultural management and nutrient-cycle representations to better resolve short-term management perturbations and event-driven export responses (https://www.innowater.com.cn/product_list_1_3.html).

Specifically, fertilization schedules can be prescribed at the HRU/field scale with hourly resolution, which improves the model's ability to reproduce rainfall-triggered export pulses following fertilization events. The model also allows dynamic adjustment of the effective wash-off soil-layer thickness and associated wash-off calculations, and it represents background pollutant pools in near-surface soils to sustain baseline runoff concentrations even in the absence of recent applications. In addition, pollutant accumulation and decay associated with plant uptake and microbial processes are parameterized using first-order kinetics, and the model represents interactions across the "soil–interflow–groundwater" continuum by allowing subsurface concentrations to respond to infiltrating inputs. Collectively, these features provide a more internally consistent depiction of nutrient mobilization, transport, and attenuation across runoff,

erosion-associated export, and leaching pathways under scenarios involving rotation, fallow, fertilization, and irrigation. InteliWay-WS produces, for each HRU and subwatershed, time series of streamflow contributions, percolation/leakage, and associated loads of TN, TP, CODCR and related indicators, which serve as boundary inputs for the groundwater and lake modules.

Groundwater processes were simulated using InteliWay-SS3D (Beijing Innowater), a secondary development based on the open-source PIHM platform. The model discretizes the watershed using an unstructured triangular mesh in the horizontal domain and vertically layered elements to represent soil and aquifer profiles, enabling three-dimensional distributed simulation of watershed water flow. InteliWay-SS3D solves variably saturated groundwater flow coupled with river channel flow, thereby representing the continuum from rainfall infiltration through surface runoff, interflow, groundwater recharge, and groundwater discharge. To reflect key hydrogeologic characteristics of the Fuxian Lake watershed and to improve the representation of river–lake exchanges, additional process modules were incorporated. Seepage-control boundary conditions were imposed on selected irrigation canals and river reaches to reflect the effects of canal lining on surface-water/groundwater interactions. A lakeshore exchange module was implemented to represent nearshore groundwater–lake interactions and to quantify groundwater discharge entering the lake along the shoreline. The coupled water-balance equations for land-surface elements and river elements are solved using an implicit scheme with adaptive time stepping to ensure numerical stability and convergence in multi-year continuous simulations. Model outputs include groundwater heads, lateral subsurface fluxes, baseflow exchanges with river reaches, and groundwater inflow to the lake. When combined with groundwater quality monitoring, these outputs enable estimation of groundwater-borne nitrogen and phosphorus loads delivered to the lake.

Lake hydrodynamics and water quality were simulated using IWIND-LR (Beijing Innowater), a secondary development based on the EFDC hydrodynamic–water quality model. IWIND-LR integrates three-dimensional hydrodynamics, water quality, and aquatic ecological processes to represent thermal stratification, circulation, and nutrient–algae dynamics, as well as the transport and transformation of TN, TP, CODCR and related indicators. The model solves the three-dimensional momentum and advection–diffusion equations using a finite-difference scheme, and incorporates external loading, sediment–water interactions (deposition/resuspension), and algal growth and mortality dynamics. For deep, oligotrophic systems such as Fuxian Lake, the framework includes nutrient-limitation functions under low background concentrations and a sediment–water exchange module to represent internal nutrient release. The horizontal grid is configured to accommodate complex basin morphology, and vertical layering is implemented with sigma coordinates to represent deep basins and irregular shorelines. IWIND-LR is forced by hourly inflow discharge and pollutant loads supplied by the watershed and groundwater modules, including inflows and TN, TP and CODCR concentrations for the eight major tributaries as well as lakeshore groundwater inflow fluxes and concentrations. Lake-surface evaporation and precipitation, together with the outflow river, are included in the lake water balance. Model outputs include time series of lake nutrient concentrations and water-quality states under alternative management scenarios, and can be extended to additional indicators such as transparency and chlorophyll-a where required.

Figure 3 conceptualizes the coupled mechanism represented by the integrated framework. InteliWay-WS simulates runoff generation and non-point load production at an hourly time step and routes discharge and associated TN, TP, CODCR loads to the river network. InteliWay-SS3D represents unsaturated-zone infiltration, three-dimensional groundwater flow, and groundwater discharge to rivers and the lake. Groundwater discharge to river reaches sustains baseflow and can

elevate dissolved nutrient concentrations, while nearshore groundwater discharge provides a direct subsurface input to the lake that is not mediated by surface channels. Together, the watershed and groundwater modules determine the time series of total inflow volume and pollutant loads to the lake, which are then used as boundary conditions for IWIND-LR. The lake model simulates dilution, transport, and biogeochemical transformation, thereby producing dynamic responses of lake nutrient concentrations and overall water-quality states. By linking source processes in the watershed to lake endpoints through explicit surface and subsurface pathways, this coupled framework enables a consistent, process-based assessment of fallow measures in terms of both load reduction and lake water-quality improvement.

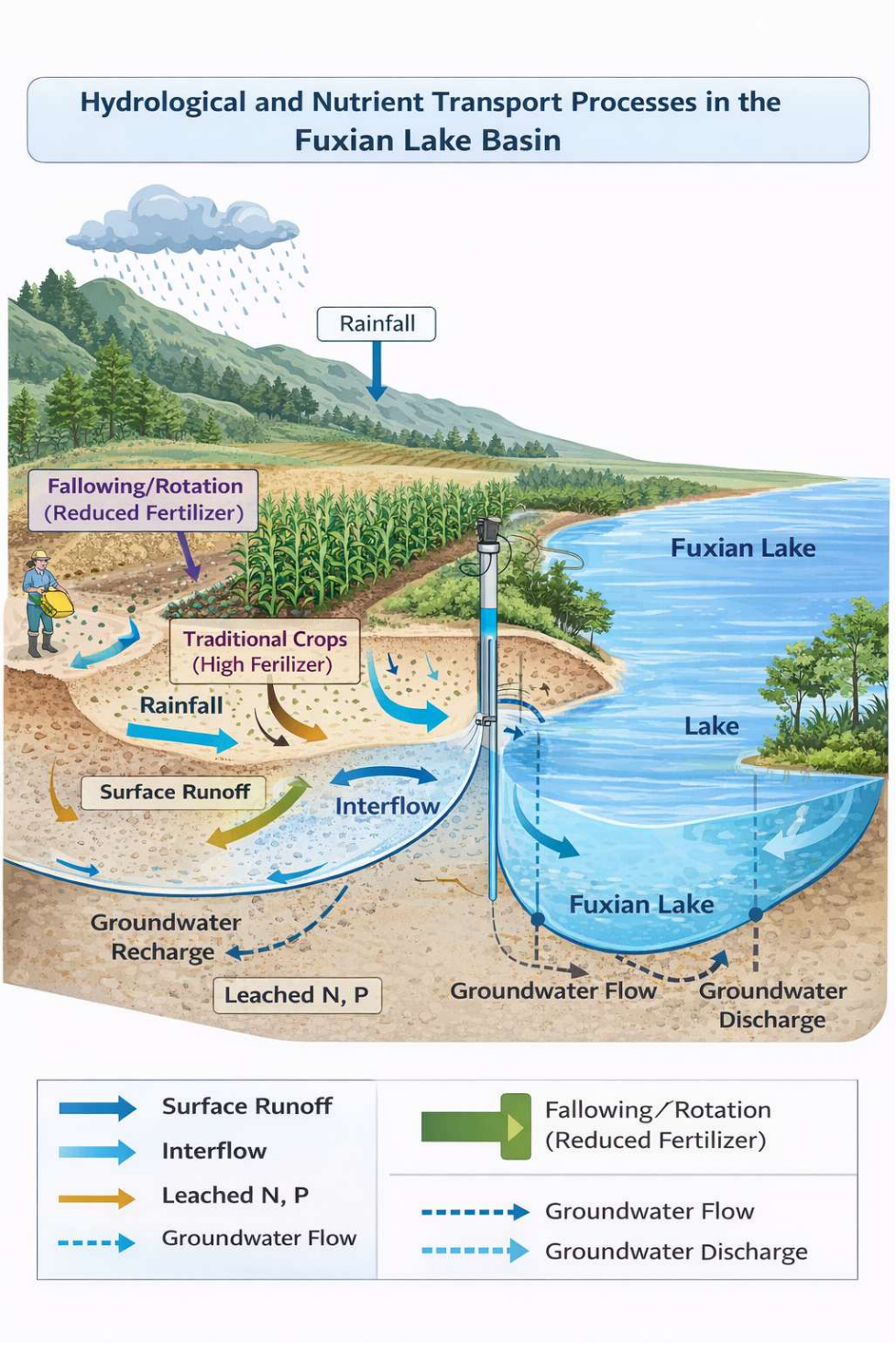


Figure 3. The coupled mechanism represented by the integrated framework

2.3 Model Calibration and Uncertainty Analysis

Before applying the models, sensitivity analysis, calibration, and uncertainty evaluation were conducted for key parameters. We employed the Morris screening (elementary effects) method to

test parameter sensitivity by perturbing individual parameters within prescribed ranges (e.g., ±10% or ±20% of initial values) and evaluating their impacts on key outputs such as annual river runoff volume, nitrogen/phosphorus loads to the lake, and groundwater heads. A set of highly sensitive parameters was identified based on these analyses (Biagi et al., 2022; Sharma et al., 2023).

For these sensitive parameters, Bayesian Optimization was applied for automated calibration. Bayesian optimization uses a Gaussian Process surrogate model to represent the parameter–objective function relationship and employs an Expected Improvement (EI) acquisition function to efficiently search the parameter space, improving convergence speed and global optimization performance. A composite objective function was constructed by weighting statistical metrics such as the Nash–Sutcliffe efficiency (NSE) coefficient and correlation coefficient. Historical observations were used to calibrate the models and obtain optimal parameter values and their posterior distributions. Key calibration parameters and ranges are summarized in Table 1.

Table 1 Key calibration parameters and their value ranges for the InteliWay-WS model

Parameter	Physical meaning	Perturbation range
LZSN	Represents the nominal water-holding capacity of the lower soil zone (i.e., the deeper root-zone/soil reservoir) that controls how much water can be stored before contributing to groundwater recharge/baseflow.	3~15
UZSN	Represents the nominal storage capacity of the upper soil zone (near-surface layer) that must be satisfied before generating significant surface runoff or transmitting water to deeper zones.	0.5~1.5
INFILT	Controls the maximum infiltration rate/capacity of the soil surface in PERLND.	0.2~4
LZETP	Controls the fraction/availability of potential ET that can be withdrawn from the lower soil zone, i.e., how strongly deep soil moisture can support evapotranspiration when the upper zone is dry.	0.1~0.9
AGWETP	Controls evapotranspiration losses directly from the active groundwater storage (i.e., baseflow reservoir) when the water table is sufficiently shallow.	0.001~0.4
eggcrate	Coefficient controlling the increase in constituent concentration in groundwater runoff induced by soil leaching, as a function of soil concentration and percolation amount; unit: 1/(d·inch).	0~0.5

Parameter	Physical meaning	Perturbation range
alpha	Surface-runoff depth required to wash off 50% of potentially removable surface constituents (*not applicable to impervious land segments*); controls the shape of the wash-off curve; unit: m.	0.005~0.1
beta	Adjustment coefficient (*not applicable to impervious land segments*), typically used as an exponent together with *alpha* to control the curvature of wash-off as runoff varies; dimensionless.	0.1~5
sqodep	Maximum soil depth that can be scoured within one hour; unit: m.	0.001~0.01
wsqop	Surface runoff rate required to remove 90% of accumulated surface constituents; unit: inch/h.	0.1~5

Calibration used 2014 to 2017 as the calibration period and 2018 to 2020 as the validation period. The InteliWay-WS watershed model was calibrated using monthly mean flows and TN/TP observations from the eight major inflow rivers. The InteliWay-SS3D groundwater model was calibrated against groundwater heads from the monitoring wells and water-level data from selected river reaches. The IWIND-LR lake model was calibrated and validated using observed lake water levels, vertical temperature profiles, TN and TP concentrations at different depths in the lake center, Secchi depth (transparency), and chlorophyll-a. After parameter optimization, discrepancies between simulated and observed outputs (e.g., inflow discharge and pollutant loads, groundwater head dynamics, and lake nutrient concentrations) were substantially reduced, and evaluation metrics reached "good" or better levels commonly accepted in practice, supporting subsequent scenario simulations.

2.4 Scenario Design and Construction of Model Inputs

To systematically evaluate the water-quality benefits of different fallow/rotation strategies, we designed one baseline scenario and multiple agricultural management scenarios (Table 2): Baseline scenario (No Fallow): No fallow implementation, representing conventional farming. Land use and cropping structure remain consistent with 2014–2017, and the same management continues

through 2018–2020 as the reference for comparison. Seasonal fallow scenarios: One season within the annual cropping system is assigned as fallow. Summer fallow: No crop during the wet season (May–September; typically the main growing season), leaving fields fallow. Winter fallow: No crop during the dry season (November to March of the following year; the minor season). Cropping in the remaining seasons follows conventional practices. Alternating-year rotation fallow scenario: A biennial rotation where each field is fallowed for a full year every two years. In the simulation period, all cropland is fully fallowed in even years (e.g., 2018 and 2020) and returns to normal cultivation in odd years, representing a possible alternate-year rotation system.Spatially targeted fallow scenarios: Selective fallow implementation based on cropland type, applied continuously throughout the simulation years, including three sub-scenarios: Paddy-field fallow: Only paddy fields are fully fallowed; dryland remains cultivated.Dryland fallow: Only dryland is fully fallowed; paddy fields remain cultivated. Whole-cropland fallow: All cropland is fully fallowed. Intensity-variant scenarios: Scenarios that differ in fallow duration and spatial coverage.Scaling-up scenarios: gradual expansion of fallow area to assess the effects of policy intensity (fallow proportion) on load reductions.

Table 2 Summary of agricultural non-point source control measures

Control Measure	Scenario Name	Fertilization Rate (kg/mu/year) TN	Fertilization Rate (kg/mu/year) TP	Fertilization Timing (Month) TP	Crop Type
Fertilization Timing	Uniform Fertilization	43.5	10.35	1~12	Vegetables
	Concentrated Fertilization	43.5	10.35	5, 11	Vegetables
Chemical Fertilizer Reduction	20% Reduction	34.8	8.28	5~8, 11~1	Vegetables
	40% Reduction	26.1	6.21	5~8, 11~1	Vegetables
	60% Reduction	17.4	4.14	5~8, 11~1	Vegetables
	80% Reduction	8.7	2.07	5~8, 11~1	Vegetables
Crop Type	Tobacco	5	2.5	5~8	Tobacco
	Rapeseed	18	5	5~8, 11~1	Rapeseed
	Maize	15	5	5~8, 10	Maize
Fallow Timing	Fallow in Main Growing Season	17.3	4.1	11~1	Vegetables
	Fallow in Off-Season	26.3	6.2	5~8	Vegetables
	Alternate-Year Fallow	43.5 / 0	10.35 / 0	5~8, 11~1	Vegetables
Fallow Spatial Pattern	Paddy Field	43.5	10.35	5~8, 11~1	Vegetables
	Dryland	43.5	10.35	5~8, 11~1	Vegetables
	Farmland	0	0	5~8, 11~1	Vegetables
	Baseline	43.5	10.35	5~8, 11~1	

To implement these scenarios, cropping and fertilization management parameters were modified accordingly. In a GIS environment, a field-parcel-based cropping structure database was established, and fallow policy information was overlaid on the 2017 baseline land-use map to generate scenario-specific spatiotemporal land-use/cropping distributions. For seasonal fallow scenarios, field parcels in the designated fallow season were assigned a "fallow" vegetation type, and fertilization and irrigation operations during that period were removed to reflect the absence of cropping and nutrient inputs. For the alternating-year scenario, planting and fertilization operations were disabled for all cropland in 2018, 2020, and other designated years. For paddy- or dryland-targeted scenarios, management operations were suspended only for the corresponding cropland type via land-use filtering.

These implementations allowed the temporal reduction and spatial contraction of nitrogen/phosphorus source strength under different fallow strategies to be represented explicitly in the models. Meanwhile, changes in evapotranspiration and surface cover conditions on fallow land were also considered—for example, representing fallow parcels as bare land or naturally grassed land to capture linked effects on runoff and erosion processes. To ensure scientific comparability across scenarios, all simulations used the same meteorological forcing as the baseline; differences among scenarios were attributable only to fallow management. After each scenario simulation, annual total inflow loads (TN, TP, CODCR) for 2018–2020 were extracted and summarized, together with percentage reductions relative to the baseline. These outputs were used to compare the effectiveness of different fallow strategies and diagnose sources of differences. By integrating high-frequency monitoring data to verify the plausibility of model outputs, we evaluated the pollution reduction and water-quality improvement benefits of fallow/rotation measures in the Fuxian Lake watershed, providing a scientific basis for optimizing agricultural non-point source pollution control policies in the region.

3 Results

3.1 Model performance: simulated versus observed runoff and water quality

Model performance was assessed using two complementary evaluation windows that align with the project implementation timeline. The period 2014 to 2017 represents the pre-fallow baseline, before the large-scale fallow and rotation measures were implemented. This baseline window is used for runoff validation at the monitored river and ditch outlets, and it also provides a reference for inflow load accounting. The period 2018 to 2020 represents the post-fallow implementation stage, during which fallow and rotation were actively applied in designated areas. Water quality evaluation therefore spans both windows, so that the model can be checked against observed concentrations before and after policy implementation, while maintaining consistent process representation.

Figures 4 jointly summarize the model performance and the seasonal characteristics of total inflow discharge to the lake for the pre-fallow (2014–2017) and post-fallow (2018–2020) periods. The continuous time-series comparison (Sim as lines; Obs as points) indicates that the model captures the dominant intra-annual hydrological cycle, with low and relatively stable flows in the dry season (Nov–Apr) and markedly elevated, event-driven flows in the wet season (May–Oct). In the pre-fallow period, observed wet-season events include several short-duration, high-magnitude peaks (reaching ~19 in the dataset units) that are not fully reproduced by the simulation. Simulated peaks are generally lower (often <~8), implying that the model underestimates the most intense runoff responses even when the seasonal timing of wet-season rising limbs is broadly consistent. In the post-fallow period, the model continues to reproduce the seasonal clustering of high flows in the wet season and the recession toward near-baseflow conditions during the dry season;

nevertheless, mismatches remain most pronounced during wet-season peak periods, when observed variability increases and the simulation tends to smooth or damp extreme responses.

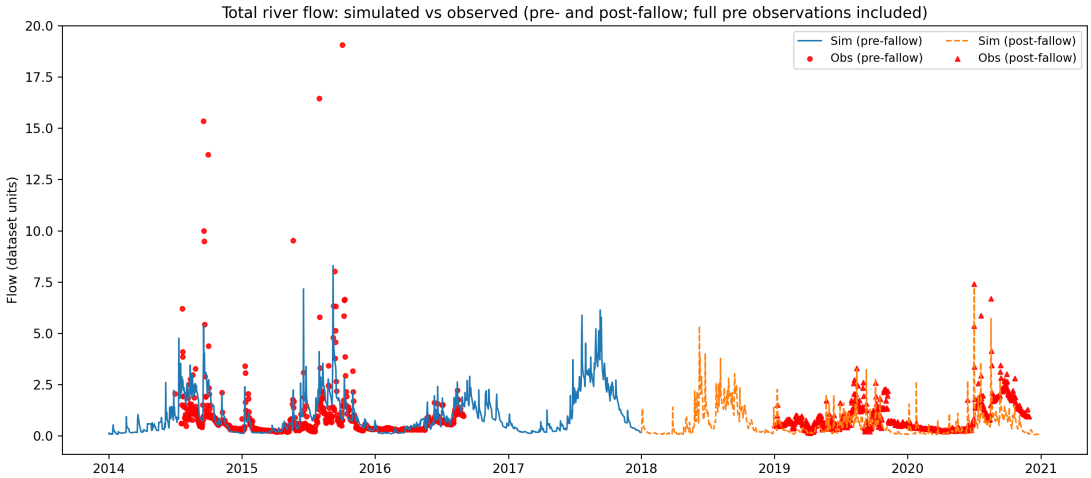


Figure 4. Comparison of simulated and observed values before and after fallow implementation (2014-2020)

In Figure 4, peak flows are concentrated in mid-year months, and the model reproduces the timing of most peaks but can overpredict or underpredict individual events at some outlets. This behavior is consistent with uncertainties in rainfall spatial heterogeneity, small-scale hydraulic structures, and rapid hillslope to channel connectivity during intense storms. By contrast, during dry-season conditions the simulated runoff remains close to zero for many days and generally matches the observed low-flow regime, but small relative biases become more visible because the denominator flow is small. This dry-season behavior is important for load assessment because low-flow periods can sustain background nutrient delivery through groundwater and near-channel seepage, even when surface runoff is limited.

Beyond model–data agreement, the time series also reveals clear pre–post differences in flow regime, especially in the timing and magnitude of wet-season pulses. Relative to the pre-fallow period, the post-fallow record shows a longer segment of sustained low-to-moderate flows

punctuated by episodic peaks, with the most prominent peaks concentrated toward the later wet-season portions of the post period. In contrast, the pre-fallow period exhibits several exceptionally large and abrupt spikes during the wet season that dominate the upper tail of the observed distribution, suggesting stronger or more abrupt runoff generation under certain storm sequences prior to fallow. Consistent with this visual impression, the seasonal error diagnostics (Figure 5) indicate that the model's systematic underestimation is a persistent feature across seasons and periods, but its magnitude changes with fallow. In the dry season, performance improves substantially from pre- to post-fallow, with NSE increasing from −1.26 to 0.47 and RMSE decreasing from 0.50 to 0.26, while the negative bias is reduced (PBIAS improves from −55.0% to −35.7%). This pattern suggests that after fallow the model tracks dry-season flow variability more reliably and with smaller absolute errors, even though it still tends to underestimate dry-season discharge on average.

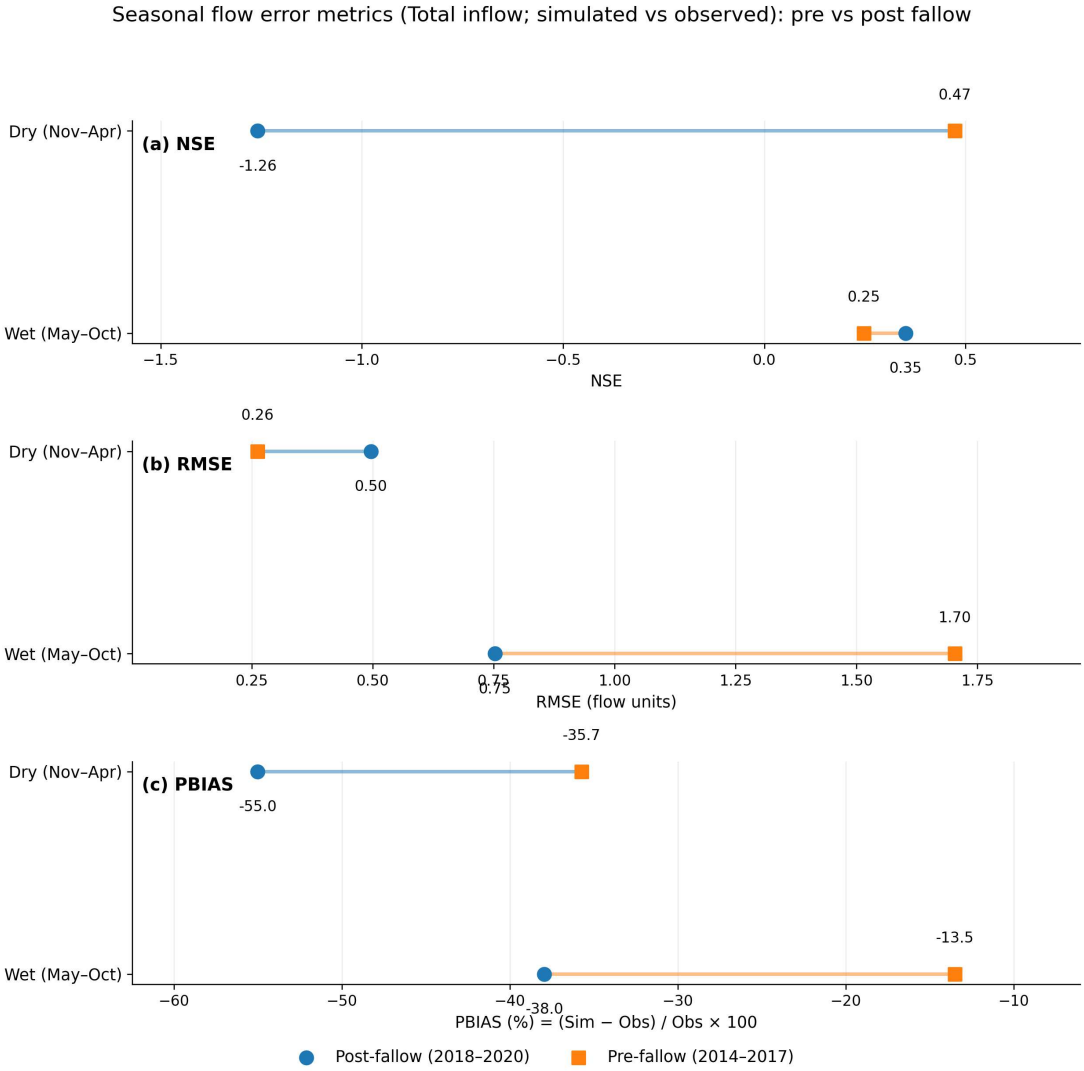
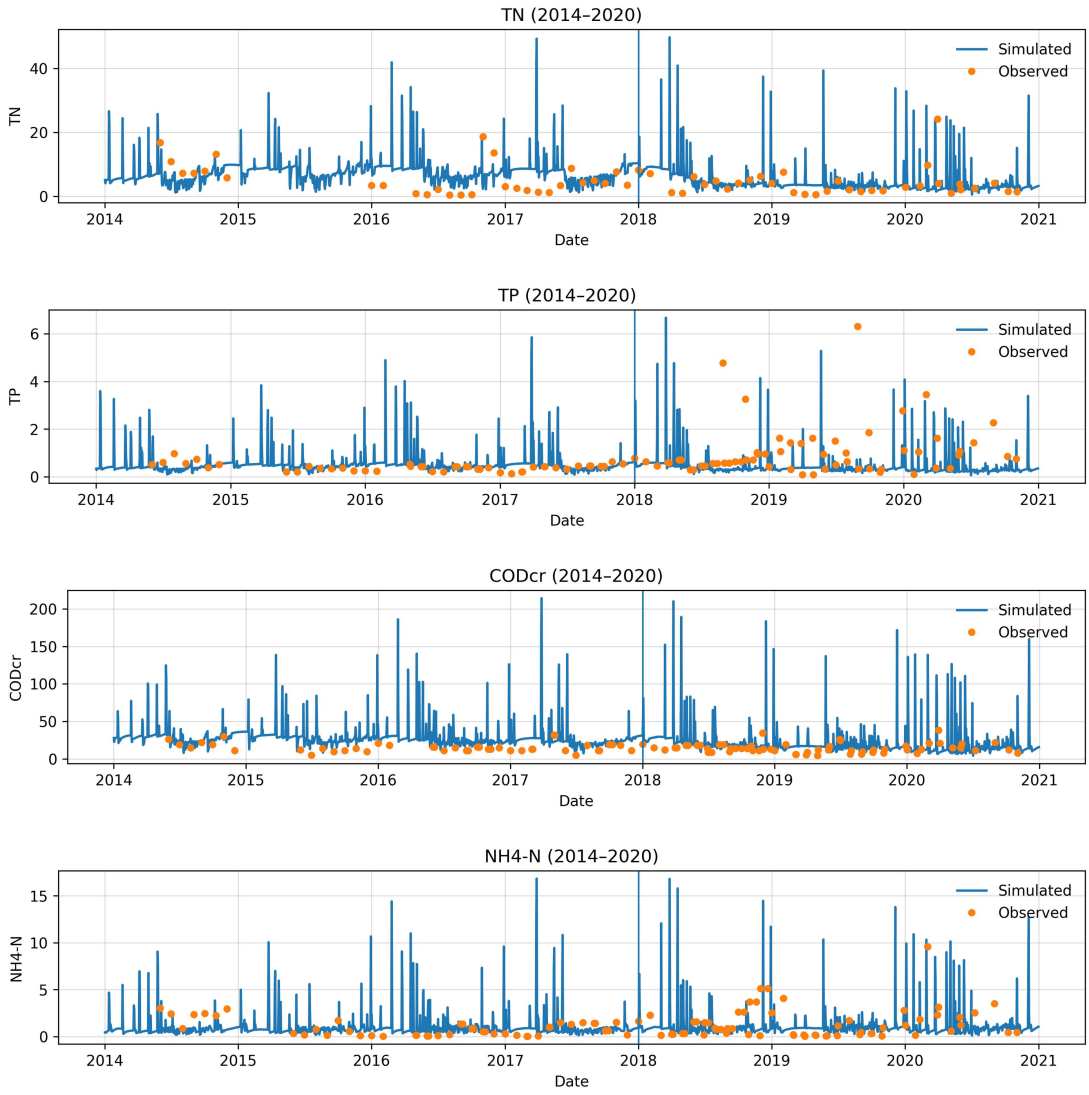


Figure 5. Comparison of key error parameters in dry and wet seasons before and after fallow implementation for flow

In the wet season, the effect of fallow is more nuanced and directly relevant to interpreting pre–post differences in inflow magnitude. The bias becomes much smaller in the post-fallow period (PBIAS improves from −38.0% to −13.5%), indicating that the simulated wet-season mean level is closer to the observations after fallow than before fallow. At the same time, wet-season error magnitude increases (RMSE rises from 0.75 to 1.70, with NSE decreasing slightly from 0.35 to 0.25), implying that the post-fallow period contains larger event-to-event deviations between

simulated and observed flows even though the average bias is reduced. In practical terms, this means that the model is closer to the observed wet-season "baseline" after fallow but is less consistent in reproducing the amplitude of individual storm-driven peaks and recessions.

Meanwhile, we evaluated the accuracy of the pollution load simulation. In Figure 6 (example monitoring section), the simulated concentrations (lines) and observed measurements (points) show a clear wet season signal (May to Oct) across all four indicators, with abrupt increases and short lived peaks that coincide with the high runoff period, followed by comparatively stable low values during the dry season (Nov to Apr). TN and TP both exhibit pronounced event scale amplification during wet months, while remaining near a low baseline for long dry season intervals. CODCR shows the strongest peakiness, with sharp rises during wet season episodes and rapid recession afterward. NH_4-N follows a similar seasonal pattern but with a generally lower baseline than TN. The pre-fallow segment (2014 to 2017) contains more frequent and higher amplitude excursions in several years, whereas the post-fallow segment (2018 to 2020) tends to show a lower background level and fewer extreme observed peaks for nitrogen species, consistent with a reduced source strength and weaker delivery connectivity after fallow implementation. Across indicators, the simulations capture the timing of most major rises and recessions, but the largest mismatches concentrate in wet season peak periods, when observed points represent discrete sampling snapshots while the model produces continuous dynamics, making peak magnitude alignment more difficult.



505

506 Figure 6. Time-series variations of water quality parameters (TN, TP, CODcr, NH_4-N) from 2014
507 to 2020

508

509 The seasonal behavior and bias patterns also differ among rivers, which helps explain why the
510 overall seasonal error metrics show strong variability (Figure 7). For TN, wet season
511 underestimation was evident in several rivers in the pre-fallow period, such as Dongdahe (PBIAS
512 -10.2% wet, 16.9% dry) and Liangwanghe (PBIAS -4.5% wet, 48.6% dry), indicating that baseline
513 and peak representation can shift between seasons even within the same river. After fallow
514 implementation, some rivers show a tendency toward higher simulated TN relative to observations

during wet months, for example Fuchenghe (PBIAS 30.4% wet) and especially Jianshanhe (PBIAS 275.6% wet and 432.3% dry), while other rivers remain closer to neutral or still underestimate in wet season, such as Dongdahe (PBIAS -28.2% wet). TP shows the most consistent cross river contrast between periods: several rivers exhibited positive bias before fallow, particularly in the dry season, for example Dongdahe (PBIAS 116.0% dry, 40.6% wet) and Liangwanghe (PBIAS 239.3% dry, 126.4% wet), whereas post-fallow TP became strongly underestimated in the wet season across multiple rivers, including Dongdahe (PBIAS -85.0% wet), Liangwanghe (PBIAS -89.6% wet), and Fuchenghe (PBIAS -70.1% wet). For CODCR, the bias direction is more river specific: Dongdahe shifted from wet season overestimation before fallow (PBIAS 86.4% wet) to underestimation after fallow (PBIAS -22.5% wet), while Liangwanghe transitioned from strong overestimation pre-fallow (PBIAS 120.6% wet and 124.1% dry) to near neutral or negative bias post-fallow in the dry season (PBIAS -35.1% dry). NH4-N also shows substantial river dependence, with Jianshanhe exhibiting very large positive bias after fallow (PBIAS 179.0% wet and 275.5% dry), while Dongdahe shifted toward mild underestimation in both seasons post-fallow (PBIAS -23.5% wet and -6.1% dry).

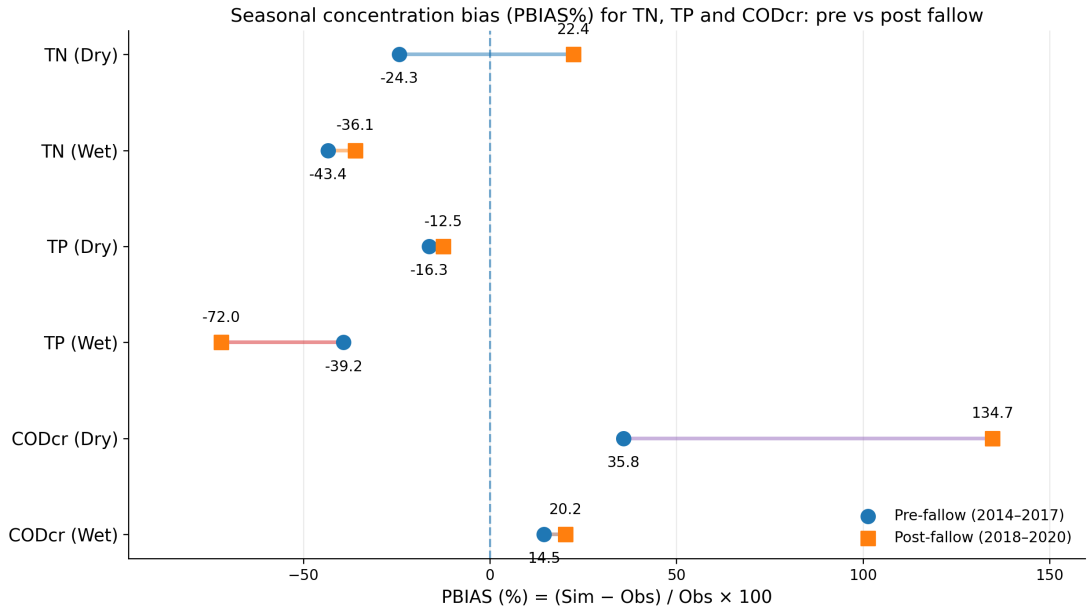
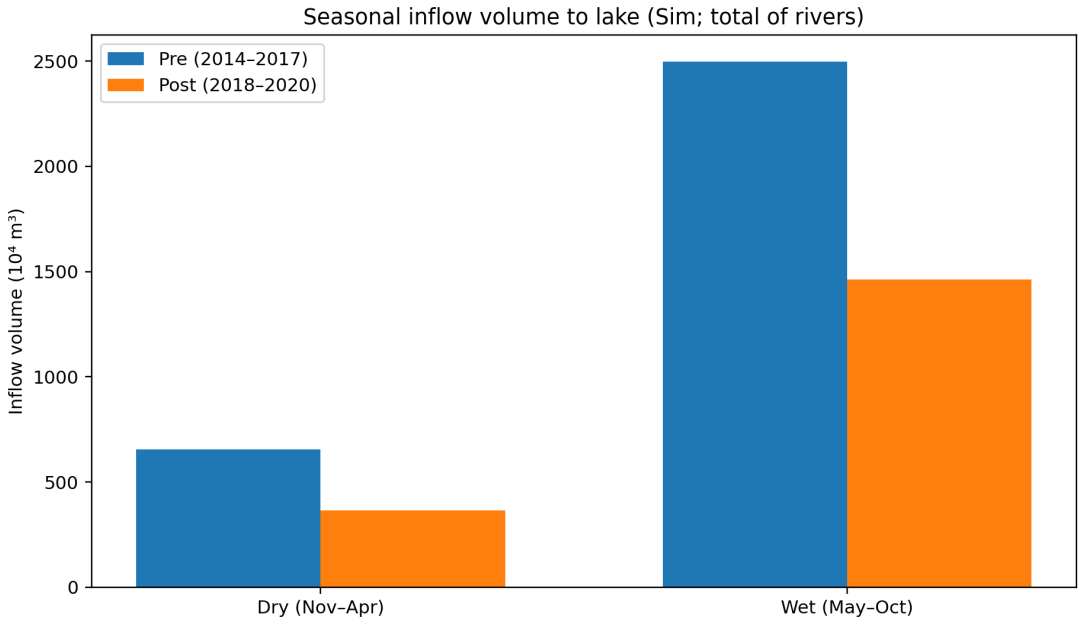


Figure 7. Comparison of key error parameters in dry and wet seasons before and after fallow implementation for TN, TP and CODCR

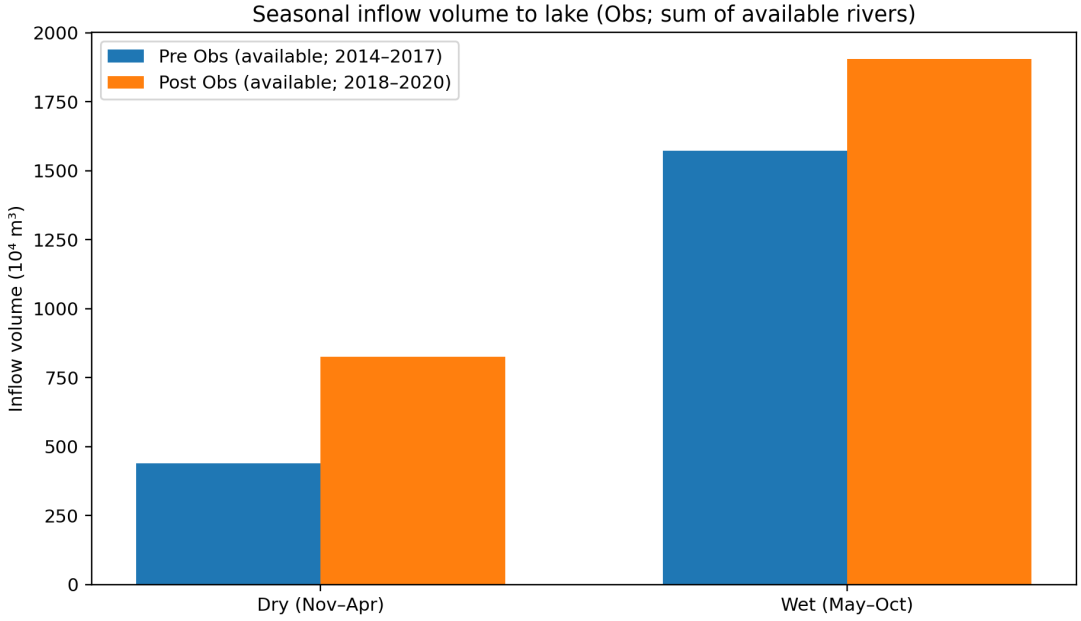
3.2 Pre and post fallow changes in inflow loads and pathway contributions

Seasonal totals further clarify how inflow volumes changed after fallow. For river (runoff) inflow, both simulation and observations consistently indicate that the wet season contributes the majority of annual inflow, reflecting the monsoon-driven hydrologic regime (Figure 8). However, the two data sources imply different pre–post directions. In the simulated totals, post-fallow seasonal inflow volumes are lower in both dry and wet seasons, indicating an overall reduction in runoff delivery to the lake during 2018–2020 relative to 2014–2017. This reduction is most consequential in the wet season because wet-season flows dominate the annual water budget; even moderate proportional decreases translate into large absolute declines in seasonal inflow volume (Figure 8.a). In contrast, the observed seasonal totals (computed as the sum of available river observations and therefore sensitive to monitoring completeness) suggest that post-fallow inflow volumes are higher, with the increase being more apparent in the dry season and a smaller but still positive change in the wet season. This pattern is consistent with the time-series comparison, which shows a denser cluster of measurable flows outside of the most intense wet-season peaks in the post-fallow period, even though peak magnitudes can still be event-driven and intermittent (Figure 8.b).

(a) Simulated seasonal inflow volume (total of rivers)



(b) Observed seasonal inflow volume (sum of available rivers)



551

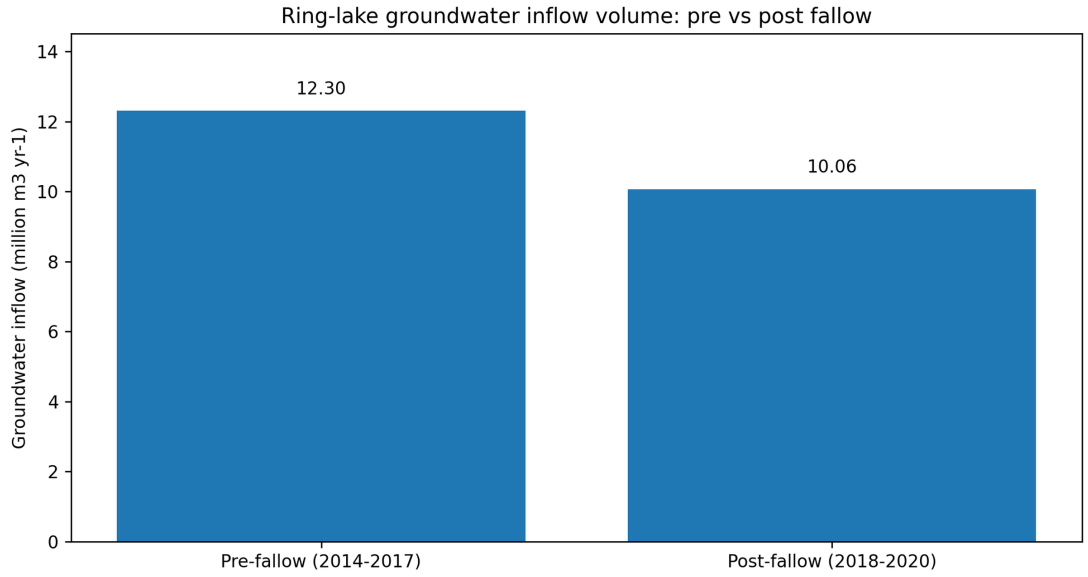
552 Figure 8. Seasonal lake inflow volume before and after fallow: simulated totals and observed, (a)
553 total of the rivers and (b) summary of the available rivers.

554

555 For groundwater inflow, the pre–post signal is clearer because it is derived from a continuous
556 monthly series (Figure 9.a). Mean annual groundwater inflow decreases from approximately

1230×10⁴ m³ in 2014–2017 to approximately 1006×10⁴ m³ in 2018–2020, corresponding to a reduction of about 18% (≈224×10⁴ m³). Unlike river runoff, groundwater exhibits a weaker wet–dry contrast because subsurface storage and delayed drainage buffer short-term rainfall variability. In the pre-fallow period, the wet-season share accounts for only about 50–54% of annual groundwater inflow, indicating that a substantial fraction of groundwater discharge to the lake persists through the dry season. When the monthly groundwater inflow series is aggregated by season, the post-fallow decline occurs in both seasons, with a slightly larger proportional reduction in wet months than in dry months. This suggests that the reduction is not simply a seasonal redistribution but a basin-wide decrease in groundwater contribution, consistent with a lower recharge supply and/or reduced hydraulic gradients feeding the lake during 2018–2020. After rainfall normalization, the river-runoff inflow shows a pronounced decline between the two periods: the simulated total river inflow volume decreases from approximately 3.22×10⁴ m³ mm⁻¹ in 2014–2017 to 2.21×10⁴ m³ mm⁻¹ in 2018–2020, corresponding to an absolute reduction of about 1.01×10⁴ m³ mm⁻¹ (a 31.3% decrease). In contrast, the groundwater inflow exhibits only a marginal change after the same normalization: the rainfall-normalized groundwater inflow decreases by 0.0265×10⁴ m³ mm⁻¹ (≈ 265 m³ mm⁻¹), representing a 2.11% reduction.

(a) Groundwater inflow volume



(b) Groundwater pollutant loads

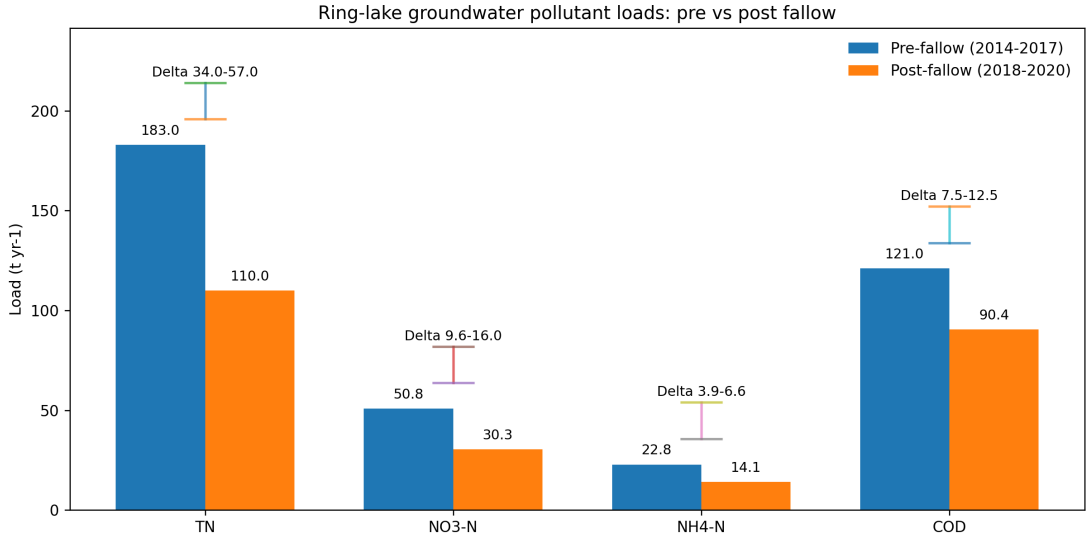


Figure 9. Ring-lake groundwater inflow and associated pollutant loads before and after fallow, (a) groundwater inflow volume and (b) groundwater pollutant loads.

To quantify how the implementation of fallow and rotation altered the delivery of pollutants to Fuxian Lake, the analysis was organized around two complementary perspectives. The first perspective focuses on total inflow loads at the watershed scale, where annual loads integrate all transport pathways and source areas. The second perspective focuses on pathway contributions, separating surface runoff, interflow, and groundwater leaching to identify how management actions

change the dominant routes of nitrogen and phosphorus export. Baseline inflow loads were characterized for 2014 to 2017 (Table 3). The mean annual loads entering the lake during the baseline period were 2601.75 t per year for CODCR, 84.13 t per year for NH_4- N, 590.48 t per year for TN, and 53.13 t per year for TP. Interannual variability is evident across 2014 to 2017, underscoring the importance of multi-year simulation for robust evaluation. Because the fallow scenarios were assessed under consistent meteorological forcing and consistent model structure, differences among scenarios can be interpreted as management driven rather than being artifacts of short-term climate anomalies.

Table 3. Baseline watershed inflow loads to the lake (2014 to 2017).

Year	COD (t/yr)	NH_4-N (t/yr)	TN (t/yr)	TP (t/yr)
2014	2698.64	78.89	552.17	49.36
2015	3147.69	86.50	698.58	65.74
2016	1941.22	81.77	478.78	43.61
2017	2619.45	89.35	632.39	53.82
Mean	2601.75	84.13	590.48	53.13

Note. Annual loads are reported in t per year. Mean values are shown for the baseline period.

The influence of fallow and rotation is particularly relevant for subsurface pathways in the ring lake zone, where shallow groundwater can directly discharge to the lake and transport dissolved nitrogen and organic matter. Figure. 9b shows both the ring lake groundwater inflow volume and the associated pollutant loads for the baseline phase (2014 to 2017) and the post implementation phase (2018 to 2020). The groundwater inflow volume decreased from approximately 12.3 million cubic meters per year to about 10.0 million cubic meters per year. Consistent with this hydrologic change, groundwater loads declined for all reported indicators. Table 3 summarizes the corresponding mean loads and reduction ranges. TN delivered by ring lake groundwater decreased

from 183.0 t per year to 110.0 t per year, with a reduction range of 34 to 57 t per year across hydrologic years. NO_3-N decreased from 50.8 to 30.3 t per year, while NH_4-N decreased from 22.8 to 14.1 t per year. CODCR decreased from 121.0 to 90.4 t per year, with a reduction range of 7.5 to 12.5 t per year. These values show that fallow and rotation can produce measurable improvements in groundwater mediated loading, but that the magnitude of reduction differs among constituents.

At the watershed scale, Figure 10.a and b compare annual TN and TP loads under no fallow versus fallow conditions for 2018 to 2020. Loads are consistently lower in the fallow case across the three years, indicating that the management intervention reduces export under different hydrologic conditions. The percentage reductions aggregated over short and long time scales are summarized in Table 4. Over a short term window defined as three consecutive years, the mean reduction is 4.63 percent for TN and 2.82 percent for TP. Over a longer window defined as seven consecutive years, the mean reduction increases to 15.55 percent for TN and 7.21 percent for TP.

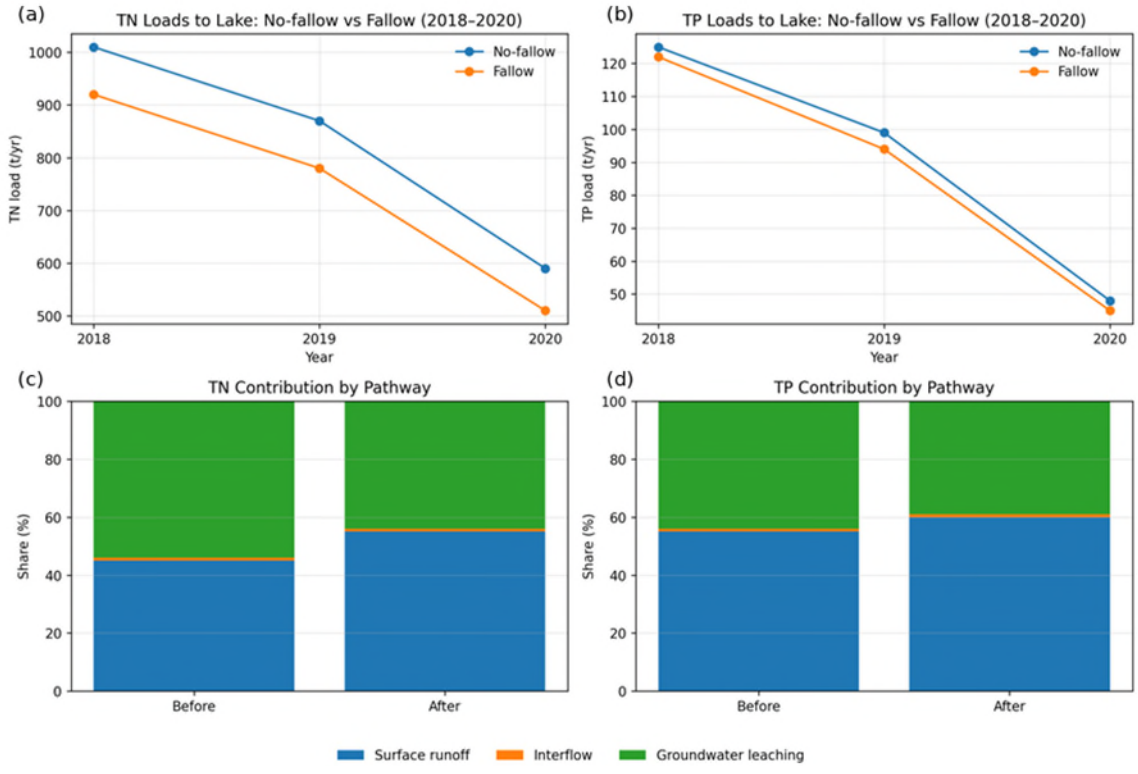


Figure 10. No-fallow versus fallow effects on lake loads and pathway contributions (2018–2020): (a) TN loads to lake under no-fallow and fallow conditions for 2018–2020, (b) TP loads to lake under no-fallow and fallow conditions for 2018–2020, (c) pathway contribution to TN export before and after fallow, and (d) pathway contribution to TP export before and after fallow.

Table 4. Ring lake groundwater loads to the lake (pre fallow versus post fallow).

Indicator	Pre-fallow mean load (t/yr)	Post-fallow mean load (t/yr)	Reduction range (t/yr)
NH_4-N	22.8	14.1	3.9–6.6
NO_3-N	50.8	30.3	9.6–16.0
TN	183.0	110.0	34–57
COD	121.0	90.4	7.5–12.5

Note. Reduction range reflects variability across hydrologic years as reported in the project outputs.

This pattern indicates that cumulative management effects and gradual adjustment of soil nutrient pools and subsurface stores can amplify benefits over longer horizons, particularly for nitrogen. The pathway contribution analysis in Figure. 10c and d provide mechanistic insight into how the fallow program changes the route by which nutrients reach the lake. For TN, the surface runoff share increases from roughly the mid 40 percent range before fallow to the mid 50 percent range after fallow, whereas groundwater leaching decreases by a similar magnitude. Interflow remains a minor component. For TP, surface runoff is the dominant pathway in both phases and increases modestly after fallow, while groundwater leaching decreases correspondingly. These shifts imply that fallow and rotation are more effective at suppressing groundwater mediated nutrient transfer than at eliminating surface driven export. In turn, this suggests that complementary measures targeting erosion control and storm runoff management remain important for controlling

TP and residual TN export from the remaining cultivated and disturbed. However, scenario specific CODCR loads across all fallow configurations were not available in the current set of scenario output tables. The results therefore support a robust conclusion on CODCR reduction for the groundwater pathway but do not permit an equally detailed comparison among all fallow scenarios for CODCR at the whole watershed scale. This limitation is addressed in the Discussion by considering constituent specific transport mechanisms and by interpreting CODCR changes primarily through hydrologic dilution and groundwater exchange pathways rather than through fertilizer management alone.

The timing results in Table 5 show that summer-season fallow achieves the strongest reductions among the timing options. TN load decreases from 682.9 t per year in the baseline to 439.4 t per year under summer-season fallow, corresponding to a 35.7 percent reduction, whereas winter-season fallow yields a 17.6 percent reduction. Biennial fallow provides intermediate performance, with a 31.4 percent reduction for TN. Across indicators, NH_4-N and TP respond similarly, with reductions around one third under summer-season fallow. Spatial targeting further changes the attainable reduction. When fallow is applied across all cultivated land, the reduction is markedly larger than when restricted to paddy fields or dryland fields only. Under the farmland-wide option, TN decreases to 325.1 t per year, a 52.4 percent reduction, and TP decreases to 31.9 t per year, a 50.4 percent reduction.

3.3 Scenario evaluation: effects of fallow timing and spatial targeting on inflow loads

Figure 11.a and Figure 11.b show the simulated annual mean loads for 2018 to 2020 under the short-term intensity scenarios. For TN, the baseline is about 550 t per year and decreases sequentially to roughly 450 t per year under short term fallow, about 400 t per year under short

term fallow plus a 10 percent cut, about 360 t per year under short term fallow plus a 20 percent cut, and about 310 t per year under short term fallow plus a 30 percent cut. For TP, the baseline is about 37 t per year and declines stepwise to about 35 t per year under short term fallow, around 31 t per year under the 10 percent cut, about 27 to 28 t per year under the 20 percent cut, and about 24 t per year under the 30 percent cut. All short-term scenarios remain below the capacity targets shown by dashed lines, with the capacity targets indicated as 648.9 t per year for TN and 40.8 t per year for TP, so the intensified scenarios further widen the margin to the target thresholds.

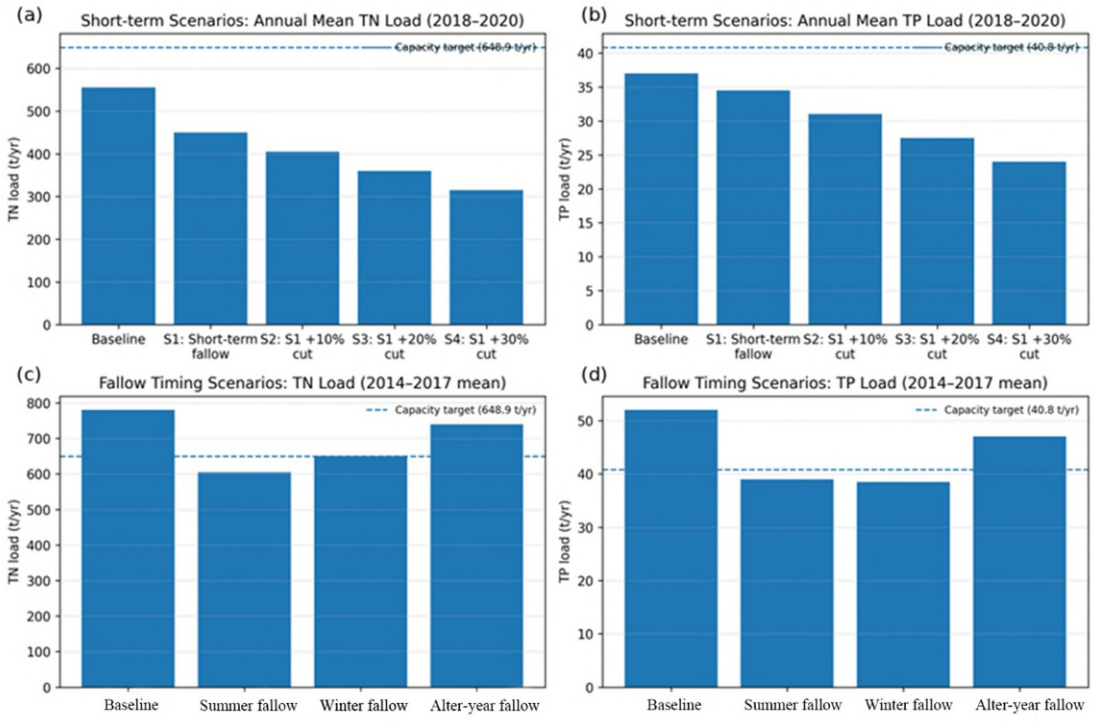


Figure 11. Scenario comparison of annual TN and TP loads under short-term reductions and fallow timing relative to capacity targets: (a) annual mean TN load (2018–2020) across short-term scenarios, (b) annual mean TP load (2018–2020) across short-term scenarios, (c) TN load (2014–2017 mean) under alternative fallow-timing scenarios, and (d) TP load (2014–2017 mean) under alternative fallow-timing scenarios.

Figure 11.c and Figure 11.d compare fallow timing strategies using the 2014 to 2017 mean loads. For TN, the baseline is about 780 t per year, summer season fallow reduces it to around 600 t per

year, winter season fallow reduces it to about 650 t per year, and alternate year rotation fallow remains high at roughly 740 t per year, which is still above the TN capacity target line at 648.9 t per year. For TP, the baseline is about 52 t per year, summer season fallow reduces it to about 39 t per year, winter season fallow reduces it to roughly 38 to 39 t per year, and alternate year rotation fallow is about 47 t per year, still above the TP capacity target line at 40.8 t per year. These panels indicate that seasonal fallow, especially summer season fallow, is more effective than alternate year rotation for bringing multi-year mean loads closer to the capacity targets.

Table 5 reports the same scenario outcomes in a structured format and adds unit area load generation for cropland. For the timing scenarios reporting loads into the lake in t per year, summer season fallow yields the largest reduction across indicators, reducing NH_4-N to 138.9 t per year, TN to 439.4 t per year, and TP to 43.8 t per year, while winter fallow yields smaller reductions and biennial fallow yields intermediate to strong reductions. For the spatial scenarios, whole cropland fallow produces the largest lake load reduction, NH_4-N to 107.2 t per year, TN to 325.1 t per year, and TP to 31.9 t per year, whereas dryland fallow consistently reduces TN and TP more than paddy field fallow. Panel C shows unit area load generation in kg per km2 per year, where the baseline unit area loads are 1170.8 for NH_4-N, 4273.4 for TN, and 445.0 for TP. Paddy field fallow reduces these to 748.0, 3151.8, and 316.1, respectively. Dryland fallow reduces them further to 491.0, 1929.0, and 238.9. Whole cropland fallow yields the strongest suppression, lowering unit area loads to 139.5 for NH_4-N, 811.8 for TN, and 137.8 for TP. These unit area results indicate that the superior performance of dryland and whole cropland fallow reflects not only reduced cultivated area but also substantially lower nutrient generation intensity per unit land area.

Table 5. Consolidated scenario outcomes for timing, spatial targeting, and unit-area cropland load generation.

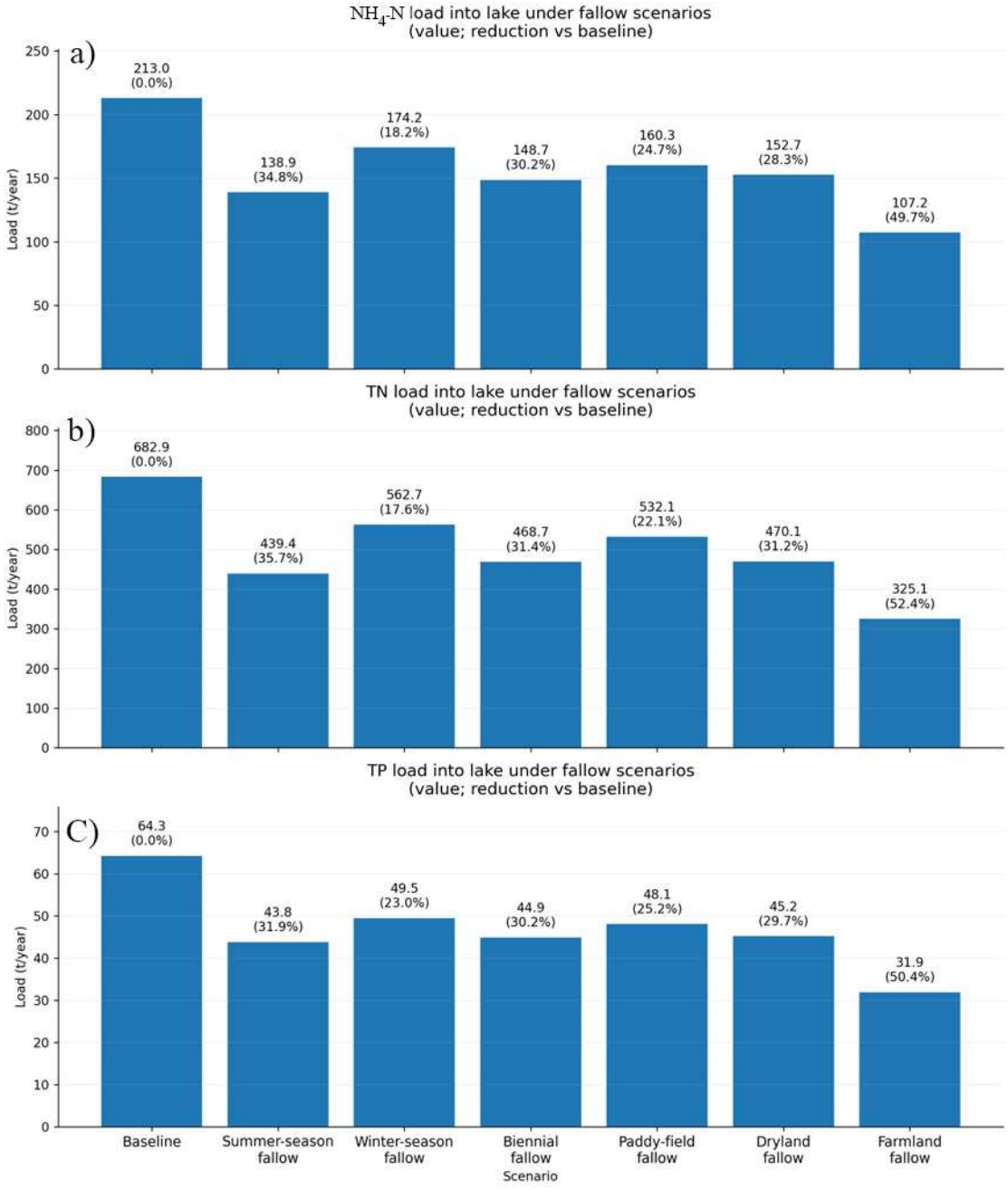
Indicator	Baseline	Summer-season fallow	Winter-season fallow	Biennial fallow
Panel A. Timing scenarios (loads into the lake, t/year; reduction vs baseline in parentheses)				
NH_4-N	213.0 (0.0%)	138.9 (34.8%)	174.2 (18.2%)	148.7 (30.2%)
TN	682.9 (0.0%)	439.4 (35.7%)	562.7 (17.6%)	468.7 (31.4%)
TP	64.3 (0.0%)	43.8 (31.9%)	49.5 (23.0%)	44.9 (30.2%)
Panel B. Spatial scenarios (loads into the lake, t/year; reduction vs baseline in parentheses)				
Indicator	Baseline	Paddy-field fallow	Dryland fallow	Farmland fallow
NH_4-N	213.0 (0.0%)	160.3 (24.7%)	152.7 (28.3%)	107.2 (49.7%)
TN	682.9 (0.0%)	532.1 (22.1%)	470.1 (31.2%)	325.1 (52.4%)
TP	64.3 (0.0%)	48.1 (25.2%)	45.2 (29.7%)	31.9 (50.4%)
Panel C. Cropland unit-				

area load generation (kg/km2/year; reduction vs baseline in parentheses)				
Indicator	Baseline	Paddy-field fallow	Dryland fallow	Farmland fallow
NH_4-N	1170.8 (0.0%)	748.0 (36.1%)	491.0 (58.1%)	139.5 (88.1%)
TN	4273.4 (0.0%)	3151.8 (26.2%)	1929.0 (54.9%)	811.8 (81.0%)
TP	445.0 (0.0%)	316.1 (29.0%)	238.9 (46.3%)	137.8 (69.0%)

Note. Panel C unit-area values are reported as kg per square kilometer per year based on typical units for cropland load generation in watershed accounting outputs

Figure 12 provides the detailed scenario comparison of loads into the lake and percent reductions relative to baseline. In the timing scenarios, NH_4-N decreases from 213.0 t per year at baseline to 138.9 t per year under summer season fallow, a 34.8 percent reduction, to 174.2 t per year under winter season fallow, an 18.2 percent reduction, and to 148.7 t per year under biennial fallow, a 30.2 percent reduction (Figure 12.a). For TN, the baseline is 682.9 t per year and decreases to 439.4 t per year under summer season fallow, a 35.7 percent reduction, to 562.7 t per year under winter season fallow, a 17.6 percent reduction, and to 468.7 t per year under biennial fallow, a 31.4 percent reduction (Figure 12.b). For TP, the baseline is 64.3 t per year and decreases to 43.8 t per year under summer season fallow, a 31.9 percent reduction, to 49.5 t per year under winter season fallow, a 23.0 percent reduction, and to 44.9 t per year under biennial fallow, a 30.2 percent reduction

(Figure 12.c). In the spatial scenarios shown on the same figure, paddy field fallow reduces NH_4-N from 213.0 to 160.3 t per year, a 24.7 percent reduction, while dryland fallow reduces it to 152.7 t per year, a 28.3 percent reduction, and whole cropland fallow reduces it to 107.2 t per year, a 49.7 percent reduction. TN declines from 682.9 t per year to 532.1 t per year under paddy field fallow, a 22.1 percent reduction, to 470.1 t per year under dryland fallow, a 31.2 percent reduction, and to 325.1 t per year under whole cropland fallow, a 52.4 percent reduction. TP declines from 64.3 t per year to 48.1 t per year under paddy field fallow, a 25.2 percent reduction, to 45.2 t per year under dryland fallow, a 29.7 percent reduction, and to 31.9 t per year under whole cropland fallow, a 50.4 percent reduction. Overall, the figure shows that summer season timing and whole cropland coverage deliver the largest absolute reductions across all three indicators, while dryland targeted fallow consistently outperforms paddy targeted fallow for TN and TP.



720

721 Figure 12. Loads into the lake under alternative fallow scenarios: a). NH_4-N, b). TN, and c). TP
722 and reductions from baseline

723

4 Discussion

4.1 Strengths of the Inteliway based modeling workflow for fallow and rotation assessment

The Inteliway-based workflow is designed as an integrated, process-based modeling system rather than a single-model application. Its main advantage for fallow and rotation assessment is that it connects management decisions at the parcel scale to load delivery at the lake boundary through explicitly coupled hydrologic and biogeochemical pathways . In the project, this integration includes a watershed hydrology and water quality model, a surface water and groundwater coupled model, and a lake hydrodynamic and water quality framework that can provide additional context for lake response. Although this paper focuses on inflow loads rather than lake water quality, the availability of lake modules strengthens the boundary conditions and supports water balance closure, which is critical when management actions alter both runoff generation and subsurface delivery over multiple years (Esselman and Stevenson, 2023).

A key innovation for representing fallow and rotation is the explicit enCODcring of seasonal crop structure and management heterogeneity at the field (or management-unit) scale. Using multi-season, multi-year planting-structure vector datasets in the fallow zone together with pre- and post-intervention fertilizer information, we constructed fertilization schedules comprising 136 distinct time-series patterns (Nouri et al., 2019). This is critical in a watershed where crop calendars and fertilizer timing govern the synchronization between nutrient availability and hydrologic transport. Conventional watershed models often rely on uniform planting calendars or simplified fertilizer timing, which can bias the simulated timing and magnitude of concentration pulses during wet-season storms. By introducing diversified rotation-specific fertilization sequences, the workflow improves the realism of source dynamics and strengthens the interpretability of scenario outcomes.

A second methodological strength is the explicit coupling of surface water, groundwater, and the downstream lake system, which is essential for the near-lake zone where shallow groundwater can exchange with channels and directly discharge to the lake. Because the ring-lake groundwater system is strongly influenced by downstream lake stage, its recharge–discharge behavior cannot be reliably characterized without representing lake–groundwater interactions. (Winter, 1999; Xu et al., 2021) We therefore implemented a coupled computational framework with a detailed discretization (7,832 triangular elements in the horizontal domain, 721 river segments, and a vertically layered configuration yielding 40,602 computational units). Hourly meteorological forcing was applied, supported by 13 rain and meteorological stations for 2014–2017 and 28 stations for 2018–2020, improving the representation of storm spatial gradients and the seasonal diagnostics reported in the Results (Pinnington et al., 2018).

The workflow further incorporated channel-type modules that distinguish ecological channels from two-side and three-side lined channels, which differ in infiltration capacity, lateral exchange, and leakage. Representing these channel classes supports a more realistic transport network from fields through drainage ditches to ring-lake groundwater pathways, improving the credibility of pathway-resolved load attribution (Čerkasova et al., 2018). Finally, to address a common challenge in inflow-load assessment—equifinality, where multiple parameter sets can reproduce river discharge while violating the lake water balance and misallocating groundwater exchange—we adopted a multi-model, multi-constraint calibration strategy. Specifically, calibration was required to satisfy consistency not only between simulated and observed river inflows, but also between simulated inflow volumes and observed lake water levels, thereby constraining the basin-scale water budget and reducing parameter non-uniqueness (Montanari et al., 2009). In addition, the coupled lake–groundwater module enables bidirectional exchange under changing hydraulic gradients; this structure provides a mechanistic basis for the ring-lake groundwater results (Figure

771 5). Importantly, water-quality consistency offers an additional cross-check: if inflow loads were
772 systematically overestimated, simulated lake concentrations would tend to exceed observations.
773 Jointly constraining water quantity and water quality through coupled calibration therefore helps
774 mitigate uncertainty arising from limited monitoring coverage and strengthens confidence in
775 scenario-based inference (Taylor et al., 2016).

776 The fallow and rotation assessment relies on the ability of the modeling workflow to represent
777 both hydrologic transport and nutrient cycling at the spatial and temporal scales that matter for
778 management. In this project, the Inteliway-WS platform was selected as the watershed hydrology
779 and water quality engine because it builds upon the LSPC lineage while being tailored for the
780 specific characteristics of the Fuxian Lake watershed and for the policy question of quantifying
781 agricultural non point source controls. A central advantage is that the platform provides a semi
782 distributed representation that is detailed enough to resolve land use and management heterogeneity
783 while remaining computationally stable for long term continuous simulation.

784 A key feature is the explicit treatment of agricultural management schedules. The fallow and
785 rotation benefit evaluation module supports fine grained representation of crop seasonal changes
786 and fertilization practices, including a large set of fertilization time series used to distinguish
787 different crop calendars and fallow windows . This capability is essential because the timing of
788 fertilizer application relative to rainfall and irrigation drives short term nutrient availability in the
789 near surface soil layer, which in turn determines the potential for wash off, runoff entrainment, and
790 leaching. Many conventional watershed models can represent fertilizer input as coarse monthly or
791 seasonal totals, but such simplification may blur the differences among management scenarios that
792 differ primarily in timing . By contrast, the Inteliway workflow enables scenario design that is
793 consistent with field surveys and parcel level planting structure, improving the realism of scenario
794 comparisons.

The modeling workflow also emphasizes process upgrades that are directly relevant to agricultural non-point source export. These include enhanced representation of fertilizer application processes, surface wash off from cropland, and the vertical migration and transformation of nitrogen and phosphorus within the soil profile . When fallow is implemented, the immediate effect is not only reduced fertilizer input but also changed soil cover and altered infiltration and runoff generation. A modeling system that can represent these coupled changes is better positioned to diagnose why load reductions differ among TN, TP, and NH_4-N, and why subsurface pathways respond differently from surface pathways (Yuning et al., 2023).

Beyond the watershed surface domain, the project integrated a coupled surface water and groundwater model using the Inteliway-SS3D platform. This platform is based on further development of the open source PIHM framework and incorporates specialized modules tailored to the basin (Song et al., 2020). Two examples are particularly relevant. First, channel lining conditions, including two side lined and three side lined channels, were represented to capture how engineered channels alter exchange between river water and groundwater. Second, explicit modules were developed to simulate dynamic exchange between surface water, groundwater, and the lake itself, which is essential in a lake basin where near shore groundwater discharge can deliver dissolved pollutants directly to the receiving waterbody (Xu et al., 2021).

Taken together, these features constitute a strength of the Inteliway based workflow for decision support. Rather than relying on a single model component, the project built a multi tiered system linking watershed runoff generation, nutrient fate and transport, and surface groundwater exchange in the ring lake zone. The evaluation against observations (Section 4.1) indicates that the framework reproduces the dominant dynamics. This provides a credible foundation for the scenario driven comparisons of fallow and rotation strategies and for interpreting the pathway level mechanisms discussed below (Gonzales-Inca et al., 2022).

4.2 Fallow reshapes pathway contributions primarily through source-input control and irrigation-mediated subsurface transfer

The pathway shifts in Figure 10 should be interpreted as the combined outcome of reduced source strength and changed irrigation-related delivery, rather than as a fundamental reorganization of catchment hydrology. The primary intervention signal is a reduction in fertilizer-driven nutrient availability: fallow and rotation lower direct N and P inputs and weaken the pool of readily mobilizable mineral N in the root zone, reducing the concentration gradients that drive downward solute transport. However, the subsurface pathway can remain non-negligible because leaching is also supported by legacy nutrient pools accumulated during long-term cultivation. Even after input reductions, stored nitrate in the vadose zone and shallow aquifer, together with continued mineralization of organic N, can sustain dissolved N export during early implementation years, which helps explain why groundwater leaching remains substantial even as its proportional contribution declines (Wu et al., 2025).

Mechanistically, nitrogen export through groundwater reflects both biogeochemical supply and hydraulic connectivity. Input reductions decrease the production and accumulation of nitrate (via reduced fertilization and altered crop uptake), while also limiting the replenishment of labile nitrate that would otherwise be flushed downward during wet periods or under irrigation. At the same time, fallow/rotation can alter the timing of nutrient availability relative to transport windows: when fertilizer pulses are reduced or shifted away from peak runoff and percolation periods, the synchronization between high nitrate availability and strong advective transport is weakened (Bourke et al., 2019). In addition, shallow groundwater nitrogen is subject to attenuation processes (e.g., denitrification) that depend on redox and carbon availability; where intermittently reducing conditions occur (common in irrigated lowlands and near-channel environments), reduced nitrate supply can amplify the effectiveness of denitrification by making nitrate the limiting reactant.

These combined mechanisms are consistent with a stronger reduction in subsurface TN loading than would be expected from water-flux change alone (Mienis and Arye, 2018).

Evidence from the near-lake system indicates that the subsurface pathway weakened in both water flux and nitrogen mass transfer. Groundwater inflow to the lake decreases from approximately 1230×10^4 m³ yr^{-1} (2014–2017) to 1006×10^4 m³ yr^{-1} (2018–2020), a reduction of about 18% ($\approx224\times10^4$ m³ yr^{-1}). After rainfall normalization, groundwater inflow decreases only slightly by 0.0265×10^4 m³ mm^{-1} (≈265 m³ mm^{-1}, 2.11%), indicating that the groundwater discharge per unit rainfall is relatively stable. In contrast, groundwater TN decreases from 183.0 to 110.0 t yr^{-1} (Table 3). This combination implies a meaningful decline in the effective nitrogen content of groundwater discharge (i.e., mass decreases more strongly than volume). As a simple diagnostic, dividing mass by discharge volume suggests an implied mean groundwater TN concentration decrease on the order of ~15 to ~11 mg L^{-1} (approximately a ~25–30% reduction), consistent with weakened leaching potential and reduced dissolved N availability in the subsurface source zone.

The hydrologic linkage most defensible for management attribution in this setting is the irrigation–drainage regime, especially in paddy-dominated systems. Irrigation and field drainage can enhance percolation and near-channel recharge, strengthening hydraulic connectivity between fields, shallow aquifers, drainage ditches, and the ring-lake groundwater system. When management shifts away from high-water-demand crops or reduces the intensity and duration of ponding and drainage, the anthropogenic recharge component can decrease, reducing the water volume available to transport dissolved N through shallow groundwater (Abbas et al., 2024; LeCoz et al., 2013). This mechanism is particularly plausible in a ring-lake zone where groundwater exchange is also modulated by downstream lake stage: lake water levels set boundary gradients

that influence whether nearshore aquifers behave as net discharge zones or exchange zones, thereby controlling the efficiency with which leached solutes are delivered to the lake. Under such conditions, source-control (less nitrate available to leach) and delivery-control (less irrigation-mediated recharge and exchange volume) act in the same direction, producing a compounded decrease in groundwater-mediated TN loading.

For phosphorus, the pathway response is expected to differ because P is more strongly retained by sorption to mineral surfaces and is frequently exported with sediment during surface runoff events. Reducing fertilizer inputs can lower dissolved reactive P availability, but the dominant TP signal at the watershed scale often remains tied to erosion, particle mobilization, and storm runoff connectivity, especially where disturbed soils, ditches, and channelized flow efficiently convey sediment to the lake. In addition, legacy P stored in topsoil can continue to supply particulate and colloidal P during intense rainfall, even when current inputs decline. These mechanisms are consistent with Figure 6 showing surface runoff as the dominant TP pathway in both phases and with a smaller long-term proportional reduction for TP relative to TN (Table 4), implying that additional sediment control and storm-runoff management are required to achieve further TP reductions beyond what source-input reduction alone can deliver.

A key interpretation of Figure 10 is that the surface-runoff share increases while total TN and TP loads decrease under fallow. Because Figure 10 reports relative shares, this pattern occurs when the groundwater component declines more strongly than the event-driven surface component: surface runoff becomes a larger fraction of a smaller total. The strong reduction in groundwater TN (Table 4), together with the modest rainfall-normalized change in groundwater discharge, supports this compositional explanation. Therefore, an increased surface-runoff share should not be interpreted as evidence that surface runoff loads increased in absolute terms; rather, it indicates

889 that subsurface improvements were proportionally stronger, leaving a residual load composition
890 that is more surface-dominated.

891 Seasonality reinforces this interpretation. Wet-season storms dominate short-duration export
892 pulses, particularly for particulate P, and are less directly controlled by fertilizer input reductions
893 alone because mobilization and connectivity can overwhelm concentration effects during extreme
894 events. In contrast, dry-season or low-flow periods emphasize slower pathways, including
895 groundwater discharge and near-channel seepage, where dissolved nitrogen transfer is more
896 sensitive to source strength and subsurface transport efficiency. Consequently, fallow and rotation
897 are expected to exert their clearest relative leverage on the subsurface nitrogen pathway, while
898 storm-driven surface export remains a key target for complementary measures focused on erosion
899 and runoff management (Nkwasa et al., 2022; Ray et al., 2015).

900 Finally, CODCR is included in the baseline and ring-lake groundwater accounting (Table 4),
901 where the groundwater-pathway response is modest. Because CODCR integrates mixed organic
902 matter sources and is not directly governed by fertilizer schedules, its change is more plausibly
903 linked to variations in groundwater exchange volume and associated dilution/processing effects
904 than to a direct reduction in an applied pollutant; hence CODCR is treated as secondary to the
905 fertilizer-driven TN/TP scenario interpretation.

906 ## 4.3 Mechanism of different fallow modes produce inflow load reductions

907 Timing scenarios differ because they modify the overlap between periods of high nutrient
908 availability and periods of high transport capacity. Summer-season fallow reduces cropping and
909 fertilization during the main rainy period, when storm runoff and erosion are most capable of
910 exporting nutrients to channels and to the lake. This reduces the coincidence of fertilizer-derived
911 nitrogen with wet-season storms, explaining why summer-season fallow yields the largest

912 reductions in Table 5. Winter-season fallow reduces inputs during a lower-transport season, so its
913 effect on annual loads is smaller even if it reduces total fertilizer application (Ramião et al., 2022).

914 Spatial scenarios indicate that effectiveness depends on both source intensity and hydrologic
915 connectivity. Paddy fields can have high nutrient loss potential due to water management, frequent
916 fertilization, and direct connection to ditch networks. Dryland fields can contribute strongly during
917 erosive events, particularly for particulate phosphorus, but annual export depends on slope, soil,
918 and proximity to channels (Yiqing et al., 2022). When fallow is applied across all cultivated land,
919 both paddy and dryland contributions are reduced and the connectivity-weighted source strength
920 decreases, producing the largest reductions.

921 Different indicators respond through different mechanisms. NH_4-N and TN are closely tied to
922 fertilizer application and soil mineral nitrogen pools, so they can respond rapidly to reduced inputs,
923 especially through leaching pathways. TP has a larger particulate component associated with
924 erosion and sediment transport, so its reduction depends more strongly on ground cover, soil
925 structure, and runoff energy. Consequently, strategies that reduce wet-season erosive transport,
926 including summer-season fallow and rotation stages that maintain cover, are particularly important
927 for phosphorus.

928 CODCR aggregates organic matter sources that include crop residues, soil organic carbon
929 mobilization, and possible non-agricultural contributions. If fallow reduces fertilizer but does not
930 strongly reduce organic matter availability or sediment-associated carbon transport, CODCR
931 reductions can be smaller. The groundwater CODCR change in Figure 9 supports this
932 interpretation, as CODCR declines but remains substantial after implementation. Achieving larger
933 CODCR reductions may therefore require complementary measures such as riparian buffer

restoration, ditch sediment management, and improved rural wastewater control in addition to fallow and rotation.

The scenario results provide a ranked portfolio that can be matched to feasibility constraints. If the objective is the largest reduction, summer-season fallow and farmland-wide targeting are prioritized. If constraints limit full-year implementation, alternate-year approaches can offer intermediate reductions. The robustness of these conclusions is strengthened by calibration across pre and post periods and by seasonal diagnostics indicating that dominant uncertainties are concentrated in storm-event peaks rather than in the annual balance. Future work can further enhance robustness by propagating uncertainty bounds and using monitoring feedback to update scenarios as implementation and farmer behavior evolve .

Timing effects are primarily governed by the coincidence of nutrient availability with transport capacity. In monsoonal climates, the wet season concentrates runoff energy and erosion potential into a limited fraction of the year. When fertilizer is applied shortly before intense rainfall, a large fraction of the applied nitrogen can remain in readily mobilized forms near the soil surface or in the shallow soil water, making it susceptible to surface wash off and leaching (Tijjani et al., 2023). Summer season fallow reduces fertilizer application during this high risk window and often increases soil cover or reduces disturbance, which decreases both the source strength and the transport efficiency. Winter season fallow, by contrast, reduces inputs during a period when runoff transport is weaker, so the marginal benefit is smaller even if fertilizer input is reduced. Biennial fallow sits between these extremes because it provides an intermittent interruption of source buildup and can reduce soil nutrient pools, but it does not consistently remove inputs during every wet season .

Spatial targeting effects are driven by heterogeneity in runoff generation, erosion, and management intensity. Paddy fields and dryland fields differ in hydrologic behavior. Paddy systems often include ponding and controlled drainage, which can attenuate runoff peaks and promote sediment settling, but can also create conditions for nutrient retention and transformation (Ray et al., 2015). Dryland fields, especially on slopes, are more directly connected to rainfall driven overland flow and rill erosion. Consequently, the unit area reductions in Table 5 indicate that dryland fallow can yield stronger relative reductions than paddy fallow on a per area basis. At the same time, paddy fields can contribute a substantial share of dissolved nutrient export through drainage and percolation when irrigated and fertilized. Therefore, the best spatial strategy is context dependent and should consider both unit area export intensity and total area.

The largest reductions are achieved under farmland wide fallow, which combines both extensive area coverage and alignment with multiple source areas. This scenario reduces TN by more than fifty percent and TP by about fifty percent relative to baseline. Mechanistically, this reflects simultaneous reduction of fertilizer inputs, reduced frequency of exposed soil surfaces, and suppression of both surface and subsurface transport from a wide range of land parcels (Pinnington et al., 2018). However, farmland wide fallow may not be feasible everywhere due to socioeconomic constraints and food production requirements. The scenario analysis therefore supports the value of hybrid approaches, where wet season fallow is prioritized in high risk sub catchments and dryland fallow is prioritized on erosion prone slopes, while paddy management focuses on drainage control, nutrient timing optimization, and near lake buffer protection .

The scenario results also illustrate that different indicators respond differently. TN shows large reductions because it is sensitive to both fertilizer input changes and subsurface transport suppression. NH_4-N reductions can be even larger than TN reductions in some spatial scenarios, reflecting its strong association with near surface source conditions and with management of

nitrogen forms. TP reductions are substantial but slightly smaller than TN in several scenarios, consistent with the persistence of erosion driven export even under fallow, particularly from legacy phosphorus stored in soils and from non agricultural disturbed land surfaces.

From a decision support perspective, the results imply that achieving targets requires both strategic timing and spatial prioritization. Figure 11 indicates that combining fallow with additional fertilizer reduction steps can move TN and TP loads closer to capacity thresholds. This suggests that fallow should be viewed as one component within a broader portfolio that includes fertilizer optimization, erosion control, drainage management, and hotspot focused interventions.

In summary, the pathway-resolved evidence supports three transferable management implications for agriculture-dominated watersheds with strong seasonality and mixed cropland types. First, to maximize short-term benefits, fallow and rotation should be aligned with periods of highest runoff risk (wet-season and storm-active months), when connectivity and transport capacity are greatest (Yuning et al., 2023). Second, to achieve deeper and more stable reductions, spatial targeting should prioritize land-use types and locations that combine high unit-area export intensity with strong hydrologic connectivity to the receiving water . Consistent with this principle, the unit-area results in Table 5 (Panel C) indicate substantially stronger per-area benefits from dryland fallow than from paddy-field fallow: for TN, dryland fallow reduces unit-area export by 54.9% (4273.4 → 1929.0 kg km^{-2} yr^{-1}), whereas paddy-field fallow reduces it by 26.2% (4273.4 → 3151.8 kg km^{-2} yr^{-1}); for TP, the corresponding reductions are 46.3% (445.0 → 238.9 kg km^{-2} yr^{-1}) versus 29.0% (445.0 → 316.1 kg km^{-2} yr^{-1}). Third, because the post-implementation pathway composition becomes relatively more surface-dominated as subsurface (groundwater) transfer is suppressed, complementary measures that directly reduce storm runoff and sediment transport remain necessary—especially for phosphorus control—so that residual event-driven export from remaining cultivated and disturbed areas can be further reduced.

Conclusion

This study developed and applied a pathway-resolved assessment to quantify how fallow and rotation reshape inflow loading to Fuxian Lake and to identify management configurations with the greatest reductions. Baseline inflow loads during 2014–2017 were substantial, with mean TN and TP inputs of 590.48 and 53.13 t yr^{-1}, respectively (CODCR 2601.75 t yr^{-1}; NH_3–N 84.13 t yr^{-1}). Against this baseline, fallow and rotation produced consistent load reductions across hydrologic years, and the magnitude of benefit increased with longer implementation horizons: mean TN and TP reductions rose from 4.63% and 2.82% over three years to 15.55% and 7.21% over seven years, indicating that cumulative adjustments in soil nutrient pools and subsurface stores can amplify benefits over time.

A key mechanism identified by the coupled accounting is the strong leverage of fallow and rotation on subsurface delivery. In the ring-lake zone, groundwater inflow declined from 12.3 to 10.0 million m^3 yr^{-1}, and groundwater-borne TN decreased from 183.0 to 110.0 t yr^{-1} (with corresponding declines in NO_3–N, NH_4–N and CODCR). This pattern indicates that management actions can measurably suppress groundwater-mediated nutrient transfer to a deep lake, which is particularly important in basins where nearshore groundwater can discharge directly to the receiving water.

Finally, the scenario analysis provides actionable priorities for management design. Timing matters: summer-season fallow delivered the largest reductions among timing options (TN −35.7%, TP −31.9%). Spatial coverage matters even more: farmland-wide fallow produced the deepest reductions (TN −52.4%, TP −50.4%), while dryland-targeted fallow outperformed paddy-only fallow in several comparisons and can be an efficient option when full-coverage implementation is

infeasible. These results support a practical hierarchy: prioritize wet-season-aligned fallow where rapid benefits are needed, expand spatial targeting toward high-export and strongly connected croplands to achieve deeper reductions, and pair fallow with storm-runoff and erosion controls to address the increasingly surface-dominated residual load structure.

Acknowledge

The authors thank the monitoring and technical staff who contributed to field data collection and model preparation.

Funding

Not applicable.

Data Availability Statement

Data Availability:

The datasets generated and/or analyzed during the current study are available from the corresponding author upon reasonable request.

Author Contributions:

Conceptualization: Rui Zou; Methodology: Tingyu Ren, Xing Chen, and Rui Zou; Data curation: Xiaolu Li, Xiaoling Zhang, and Wenjing Ma; Formal analysis: Tingyu Ren, Xing Chen, and Xiaolu Li; Writing-original draft: Tingyu Ren and Xing Chen; Writing-review and editing: Ziguan Wang,

Rui Zou; Supervision: Ziguan Wang and Rui Zou. Tingyu Ren and Xing Chen contributed equally to this work. All authors have read and approved the final manuscript.

Reference

Abbas, S.A., Bailey, R.T., White, J.T., Arnold, J.G., White, M.J., Čerkasova, N., Gao, J., 2024. A framework for parameter estimation, sensitivity analysis, and uncertainty analysis for holistic hydrologic modeling using SWAT+. Hydrol. Earth Syst. Sci. 28(1), 21–48. https://doi.org/10.5194/hess-28-21-2024

Aboelnour, M., Tank, J., Hamlet, A., Bertassello, L., Ren, D., Bolster, D., 2023. Modeling the impact of changing land use and vegetative cover on hydrology, nutrient, and sediment loads from an agricultural catchment of Lake Michigan (USA). EGU General Assembly 2023, Vienna, Austria, 23–28 April 2023, EGU23–5142. https://doi.org/10.5194/egusphere-egu23-5142

Biagi, K.M., Ross, C.A., Oswald, C.J., Sorichetti, R.J., Thomas, J.L., Wellen, C.C., 2022. Novel predictors related to hysteresis and baseflow improve predictions of watershed nutrient loads: An example from Ontario's lower Great Lakes basin. Sci. Total Environ. 826, 154023. https://doi.org/10.1016/j.scitotenv.2022.154023

Bodrud-Doza, M., Yang, W., Liu, Y., Yerubandi, R., Daggupati, P., DeVries, B., Fraser, E.D.G., 2025. Evaluating best management practices for nutrient load reductions in tile-drained watersheds of the Laurentian Great Lakes Basin: A literature review. Sci. Total Environ. 965, 178657. https://doi.org/10.1016/j.scitotenv.2025.178657

Bonab, M.H., Nayyer, S., 2020. The impact of spatial decision variables influencing crop rotation on phosphorus load reduction: A hydrologic modeling approach

Bourke, S., Iwanyshyn, M., Kohn, J., Hendry, M.J., 2019. Sources and fate of nitrate in groundwater at agricultural operations overlying glacial sediments. Hydrol. Earth Syst. Sci. 23(3), 1355–1373. https://doi.org/10.5194/hess-23-1355-2019

Čerkasova, N., Umgiesser, G., Ali, E., 2018. Development of a hydrology and water quality model for a large transboundary river watershed to investigate the impacts of climate change – A SWAT application. Ecol. Eng. 124(0), 99–115. https://doi.org/10.1016/j.ecoleng.2018.09.025

Chang, C.F., Astitha, M., Yuan, Y., Tang, C., Vlahos, P., Garcia, V., Khaira, U., 2023. A new approach to predict tributary phosphorus loads using machine learning- and physics-based modeling systems. Artif. Intell. Earth Syst. 2(3), 1–20. https://doi.org/10.1175/aies-d-22-0049.1

Chao, X., Witthaus, L., Bingner, R., Jia, Y., Locke, M., Lizotte, R., 2023. An integrated watershed and water quality modeling system to study lake water quality responses to agricultural management practices. Environ. Model. Software. 164, 105691. https://doi.org/10.1016/j.envsoft.2023.105691

Cheng, X., Dong, Y., Li, Y., Wang, S., 2025. New Source-Transfer-Sink analytical framework for dynamic tracking of nitrogen and phosphorus flows and changes in watersheds. EGU

General Assembly 2025, Vienna, Austria, 27 April–2 May 2025, EGU25–5073. https://doi.org/10.5194/egusphere-egu25-5073
Esselman, P.C., Stevenson, R.J., 2023. Model-based assessment and mapping of total phosphorus enrichment in rivers with sparse reference data. Sci. Total Environ. 884, 163418. https://doi.org/10.1016/j.scitotenv.2023.163418
Gonzales-Inca, C., Calle, M., Croghan, D., Haghighi, A.T., Marttila, H., Silander, J., Alho, P., 2022. Geospatial Artificial Intelligence (GeoAI) in the integrated hydrological and fluvial systems modeling: Review of current applications and trends. Water 14(14), 2211. https://doi.org/10.3390/w14142211
He, D., Liu, X., Fu, Y., Wang, T., Zhu, B., 2023. Field baseflow eluting SOM-rich sandy soil to exacerbate non-point source pollution of Lake Erhai, Southwest China. Horticulturae 9(8), 898. https://doi.org/10.3390/horticulturae9080898
Husk, B., Julian, P., Simon, D., Tromas, N., Phan, D., Painter, K., Baulch, H., Sauvé, S., 2024. Improving water quality in a hypereutrophic lake and tributary through agricultural nutrient mitigation: A Multi-year monitoring analysis. J. Environ. Manage. 354, 120411. https://doi.org/10.1016/j.jenvman.2024.120411
Kujawa, H., Kalcic, M., Martin, J., Apostel, A., Kast, J., Murumkar, A., Evenson, G., Aloysius, N., Becker, R., Boles, C., Confesor, R., Dagnew, A., Guo, T., Muenich, R.L., Redder, T., Wang, Y.-C., Scavia, D., 2022. Using a multi-institutional ensemble of watershed models to assess agricultural conservation effectiveness in a future climate. J. Am. Water Resour. Assoc. 58(6), 1326–1340. https://doi.org/10.1111/1752-1688.13023
LeCoz, M., Favreau, G., Ousmane, S., 2013. Modeling increased groundwater recharge due to change from rainfed to irrigated cropping in a semiarid region. Vadose Zone J. 12(2), 2–12. https://doi.org/10.2136/vzj2012.0148
Lintern, A., McPhillips, L., Winfrey, B., Duncan, J., Grady, C., 2020. Best management practices for diffuse nutrient pollution: wicked problems across urban and agricultural watersheds. Environ. Sci. Technol. 54(15), 9159–9174. https://doi.org/10.1021/acs.est.9b07511
Liu, D., Huang, L., Jia, L., Li, S., Wang, P., 2024. Evaluation of best management practices for mitigating harmful algal blooms risk in an agricultural lake basin using a watershed model integrated with Bayesian Network approach. J. Environ. Manage. 364, 121433. https://doi.org/10.1016/j.jenvman.2024.121433
Liu, Y., Yang, W., Bass, B., Rao, Y.R., 2025. Effectiveness of agricultural BMPs on phosphorus load reduction for the Canadian Lake Erie Basin: a literature review. Environ. Rev. 33, 1–24. https://doi.org/10.1139/er-2024-0069
Mehdi-Schulz, B., Moura Lima, E., Egger, C., Gaube, V., 2025. Quantifying nitrogen flows from agricultural land using an ABM to inform future land use change for ecohydrological modelling. EGU General Assembly 2025, Vienna, Austria, 27 April–2 May 2025, EGU25–12089. https://doi.org/10.5194/egusphere-egu25-12089
Mienis, O., Arye, G., 2018. Long-term nitrogen behavior under treated wastewater infiltration basins in a soil-aquifer treatment (SAT) system. Water Res. 134(1), 192–199. https://doi.org/10.1016/j.watres.2018.01.069
Miller, J.W., Karimi, K., Sankarasubramanian, A., Obenour, D.R., 2021. Assessing interannual variability in nitrogen sourcing and retention through hybrid Bayesian watershed modeling. Hydrol. Earth Syst. Sci. 25(5), 2789–2804. https://doi.org/10.5194/hess-25-2789-2021
Montanari, M., Hostache, R., Matgen, P., Schumann, G., Pfister, L., Hoffmann, L., 2009. Calibration and sequential updating of a coupled hydrologic-hydraulic model using remote sensing-derived water stages. Hydrol. Earth Syst. Sci. 13(3), 367–380. https://doi.org/10.5194/hess-13-367-2009

Mooney, R.J., Stanley, E.H., Rosenthal, W.C., Esselman, P.C., Kendall, A.D., McIntyre, P.B., 2020. Outsized nutrient contributions from small tributaries to a Great Lake. Proc. Natl. Acad. Sci. U.S.A. 117(45), 28175–28182. https://doi.org/10.1073/pnas.2001376117

Nkwasa, A., Chawanda, C.J., Jägermeyr, J., Griensven, a.A.v., 2022. Improved representation of agricultural land use and crop management for large-scale hydrological impact simulation in Africa using SWAT+. Hydrol. Earth Syst. Sci. 26(1), 71–89. https://doi.org/10.5194/hess-26-71-2022

Nouri, H., Stokvis, B., Galindo, A., Blatchford, M., Hoekstra, A.Y., 2019. Water scarcity alleviation through water footprint reduction in agriculture: The effect of soil mulching and drip irrigation. Sci. Total Environ. 653(0), 241–252. https://doi.org/10.1016/j.scitotenv.2018.10.311

Peng, J., Jin, C., Wu, Y., Hou, Z., Gao, S., Chu, Z., Zheng, B., 2022. Modeling non-point source nutrient loads with different cropping systems in an agricultural lake watershed in Southwestern China: From field to watershed scale. Mathematics 10(21), 4047. https://doi.org/10.3390/math10214047

Pinnington, E., Quaife, T., Black, E., 2018. Impact of remotely sensed soil moisture and precipitation on soil moisture prediction in a data assimilation system with the JULES land surface model. Hydrol. Earth Syst. Sci. 22(4), 2575–2588. https://doi.org/10.5194/hess-22-2575-2018

Ramião, J.P., Carvalho-Santos, C., Pinto, R., Pascoal, C., 2022. Modeling the effectiveness of sustainable agricultural practices in reducing sediments and nutrient export from a river basin. Water 14(23), 3962. https://doi.org/10.3390/w14233962

Ramião, J.P., Pascoal, C., Pinto, R., Carvalho-Santos, C., 2024. Mitigating water pollution in a Portuguese river basin under climate change through agricultural sustainable practices. Mitig. Adapt. Strateg. Glob. Change. 29(4), 25. https://doi.org/10.1007/s11027-024-10121-9

Ray, D.K., Gerber, J.S., MacDonald, G.K., West, P.C., 2015. Climate variation explains a third of global crop yield variability. Nat. Commun. 6(1), 5989. https://doi.org/10.1038/ncomms6989

Sharma, S., Bijukshe, S., Puppala, S.S., 2023. Monitoring, modeling and planning best management practices (BMPs) in the Atwood and Tappan Lake watersheds with stakeholders engagements. Water 15(17), 3028. https://doi.org/10.3390/w15173028

Song, J., Yang, Y., Sun, X., Lin, J., Wu, M., Wu, J., Wu, J., 2020. Basin-scale multi-objective simulation-optimization modeling for conjunctive use of surface water and groundwater in northwest China. Hydrol. Earth Syst. Sci. 24(5), 2323–2341. https://doi.org/10.5194/hess-24-2323-2020

Taylor, S.D., He, Y., Hiscock, K.M., 2016. Modelling the impacts of agricultural management practices on river water quality in Eastern England. J. Environ. Manage. 180, 147–163. https://doi.org/10.1016/j.jenvman.2016.05.002

Tijjani, S.B., Qi, J., Giri, S., Lathrop, R., 2023. Modeling land use and management practices impacts on soil organic carbon loss in an agricultural watershed in the Mid-Atlantic Region. Water 15(20), 3534. https://doi.org/10.3390/w15203534

Trang, N.T.N., Agnieszka, P.-L., Jolanta, D., Krystyna, M., 2025. Current challenges, methods, and strategies for reducing the transfer of nonpoint source pollution from agricultural areas to surface water J. Water Land Dev. 66(VII–IX), 187–205 https://doi.org/10.24425/jwld.2025.155314

Venishetty, V., Parajuli, P.B., To, F., Nepal, D., Baker, B., Gude, V.G., 2024. Evaluating best management practice efficacy based on seasonal variability and spatial scales. Hydrology 11(4), 58. https://doi.org/10.3390/hydrology11040058

Wan, L., Kendall, A.D., Martin, S.L., Hamlin, Q.F., Hyndman, D.W., 2023. Important role of overland flows and tile field pathways in nutrient transport. Environ. Sci. Technol. 57(44), 17061–17075. https://doi.org/10.1021/acs.est.3c03741

Wang, C., Huang, C., Zhang, S., Zhang, L., Li, T., Peng, J., Zhang, L., 2023. Research progress on nitrogen and phosphorus loss in small watersheds: A regional review. Water 15(16), 2894. https://doi.org/10.3390/w15162894

Wei, Z., Alam, S., Verma, M., Hilderbran, M., Wu, Y., Anderson, B., Ho, D.E., Suckale, J., 2024. Integrating water quality data with a Bayesian network model to improve spatial and temporal phosphorus attribution: Application to the Maumee River Basin. J. Environ. Manage. 360, 121120. https://doi.org/10.1016/j.jenvman.2024.121120

Winter, T.C., 1999. Relation of streams, lakes, and wetlands to groundwater flow systems. Hydrogeol. J. 7(1), 28–45. https://doi.org/10.1007/s100400050178

Wu, H., Chen, D., 2024. Modification of exploration of long-term nutrient trajectories for phosphorus (ELEMeNT-P) model to quantify legacy phosphorus dynamics in a typical watershed of eastern China. EGU General Assembly 2024, Vienna, Austria, 14–19 April 2024, EGU24–713. https://doi.org/10.5194/egusphere-egu24-713

Wu, H., Zhou, J., Wang, Y., Jiao, X., Pan, Z., Zhang, Y., Du, J., Zhang, Z., Ma, L., Chen, D., 2025. Modification of Exploration of Long-term Nutrient Trajectories for Phosphorus (ELEMeNT-P) model to quantify legacy phosphorus dynamics in a typical watershed of eastern China. J. Hydrol. 661, 133718. https://doi.org/10.1016/j.jhydrol.2025.133718

Xu, S., Frey, S.K., Erler, A.R., Khader, O., Berg, S.J., Hwang, H.T., Callaghan, M.V., Davison, J.H., Sudicky, E.A., 2021. Investigating groundwater-lake interactions in the Laurentian Great Lakes with a fully-integrated surface water-groundwater model(Article). J. Hydrol. 595, 125911. https://doi.org/10.1016/j.jhydrol.2020.125911

Yiqing, Y., Lund, J.R., Harter, T., 2022. Conjunctive water management for agriculture with groundwater salinity. Water Resour. Res. 58(10), e2021WR031058. https://doi.org/10.1029/2021wr031058

Yuning, S., Montes, F., Kemanian, A.R., 2023. Cycles-L: A coupled, 3-D, land surface, hydrologic, and agroecosystem landscape model. Water Resour. Res. 59(8), e2022WR033453. https://doi.org/10.1029/2022wr033453

Zhao, H., Wang, Y., Dong, Y., He, Z., Wang, P., Zheng, H., He, J., Zeng, W., 2023. Modeling the response of agricultural non-point source pollution to planting structure and fertilization level in Erhai Lake Basin under low-latitude plateau climate. Ecol. Indic. 154, 110829. https://doi.org/10.1016/j.ecolind.2023.110829

Zhou, J., Mogollón, J.M., van Bodegom, P.M., 2024. Assessing nutrient fate from terrestrial to freshwater systems using a semi-distributed model for the Fuxian Lake Basin, China. Sci. Total Environ. 921, 171068. https://doi.org/10.1016/j.scitotenv.2024.171068